PHYSICO-CHEMICAL STUDIES ON SOME IRON AND ALUMINIUM OXIDES

A thesis submitted to the University of Pune

for

THE DEGREE OF MASTER OF SCIENCE IN CHEMISTRY

(Partly by papers and partly by research)

by

A. N. KOTASTHANE
B.Sc.(Hons.)

NATIONAL CHEMICAL LABORATORY,
PUNE-411008, INDIA.

JUNE - 1978

A C K N O W L E D G E M E N T

I am indebted to Dr.(Miss) S.B. Kulkarni for her constant inspiration and guidance during the course of this investigation. I gratefully acknowledge the valuable advice and helpful suggestions given by Mr. Lakhbir Singh throughout the course of this work.

I am thankful to my colleagues and friends for their whole hearted cooperation especially for taking X-ray diffractograms and thermograms of iron and aluminium oxides.

Finally, I am grateful to the Director, National Chemical Laboratory, Pune 411008, for allowing me to submit this investigation in the form of a thesis.

(A.N. KOTASTHANE)

PUNE,
June 19, 1978.

C O N T E N T S

continued...

continued ...

P A R T - I :

CHAPTER - I : INTRODUCTION

INTRODUCTION

The common oxides of iron are ferrous oxide FeO, ferric oxide Fe_2O_3 and magnetite Fe_3O_4. Ferric oxide Fe_2O_3 normally has the triagonal corundum structure of the hexagonal system, and it is non-magnetic. However, it has now been known for many years that Fe_2O_3 can also be prepared in a magnetic form by carefully heating Fe_3O_4 in air. Welo and Baudisch[1] showed that this brownish-red "magnetic Fe_2O_3" is not merely a thin red layer of non-magnetic Fe_2O_3 over black magnetic Fe_3O_4 as was originally believed, but is a definite compound. In the X-ray studies they found no evidence for any lines corresponding to the hexagonal structure of Fe_2O_3. Nevertheless, the X-ray powder pattern of this magnetic form of Fe_2O_3 was found to be indistinguishable from that of Fe_3O_4, thus indicating a spinel structure of the cubic system. The hexagonal structure of compounds in general is designated as the alpha (α) form, and the cubic structure as the gamma (γ) form[2-5].

Iron oxides, besides showing different crystal structures and magnetic properties, also exhibit interesting variations in their colour. Ferrosoferric oxide Fe_3O_4 is black, hematite α-Fe_2O_3 is red, while maghemite (magnetic form) γ-Fe_2O_3 is brown to brownish-red in colour.

In addition to these, ferric oxide also exists in a hydrated form ($Fe_2O_3.H_2O$ or FeOOH) which exhibits a range of yellow shades. On account of their fastness and cheap availability, these iron oxides are widely used as pigments in the paint industry. For this purpose, the iron oxides have to be prepared in very fine particle size.

Ultrafine particles (0.1 μ to 10.0 μ) of a wide range of inorganic compounds are utilised extensively in protective coatings, anticorrosive paints, electronics, ceramics, plastics, paper and building materials. Historically, the pigment industry was one of the pioneers in producing fine particles. In the early stages grinding technology was used to obtain fine particles from mineral ores. As need arose for high purity and particle size consistency, different techniques were evolved in chemical industry to produce ultrafine synthetic particles. Besides control on particle size, processes have been developed to obtain particles of different shapes which are described in Chapter-II. The differences in shape enhance the utility of the powders especially of the magnetic oxides.

Magnetic iron oxides of synthetic origin are extensively used for recording purposes. The magnetic recording surface coatings on discs, tapes and cylinders usually comprise a magnetic iron oxide dispersed in resinous binder. In his review Jacob[6] has mentioned that

the concept of magnetic recording of sound or signals was first patented by Valdemar Pautsen of Denmark as early as 1890-1900. However, the first commercial magnetic recording tape similar to the present product was introduced in the market by Germany just prior to the Second World War.

Two types of magnetic iron oxide powders are used as magnetic recording media. Powders having spherical isotropic particles are termed 'equant' and those having elongated needle-shaped particles are called 'acicular'. The method of preparation of first type followed by the Germans giving spherical particles has been described by Ranger[7], comprising calcination of ferrous oxalate. Improvements on this process developed as a result of this investigation are discussed in Section-A of Chapter-II. Magnetic iron oxides obtained by this method have comparatively low coercive force in the range of 100 to 150 Oerstads, resulting in a limited utilisation of the recording media[8].

Magnetic iron oxide powders with higher coercivity and better utility result if they are obtained in the acicular form. These are prepared from ferric oxide hydrate FeOOH, by a cyclic reduction and oxidation process. This process has been the subject of extensive investigations covered by patents. The current technology and improvements on it are described in Section-B of Chapter-II.

CHAPTER - II : METHODS OF PREPARATION OF GAMMA FERRIC OXIDE

SECTION - A

FERROUS OXALATE PROCESS FOR THE PREPARATION OF 'EQUANT' GAMMA FERRIC OXIDE

2.A.1 Preparation of Ferrous Oxalate Dihydrate :

Ferrous oxalate was prepared using the method described by Robin[9]. Reagent grade chemicals namely crystalline ferrous sulphate ($FeSO_4.7H_2O$) and oxalic acid ($H_2C_2O_4.2H_2O$) were used without further purification. The solutions were prepared in double distilled water.

Ferrous oxalate dihydrate was precipitated by mixing warm equal volumes (250 ml.) of equimolar (0.5 M) solutions of ferrous sulphate ($FeSO_4$) and oxalic acid ($H_2C_2O_4$) at 60°C under vigorous stirring.

$$FeSO_4.7H_2O + H_2C_2O_4.2H_2O \longrightarrow FeC_2O_4.2H_2O + H_2SO_4 + 7H_2O \quad \ldots\ldots (1)$$

It was found that addition of ferrous sulphate solution (0.5 M) to hot solution of oxalic acid (0.5 M) resulted in a better product. The yellow crystalline precipitate thus obtained (20.384 gms.) filtered quite easily through a sintered glass funnel, and was washed with cold water two to three times and then with acetone to speed up drying. It was air-dried at the ambient temperature. The product obtained is finely divided light yellow

crystals of ferrous oxalate dihydrate ($FeC_2O_4.2H_2O$) of substantially uniform particle size in the micron range.

The product was analysed by standard analytical procedures. The ferrous oxalate content was determined by titration with $KMnO_4$, followed by estimation of resulting ferric iron with mercurous nitrate solution in presence of excess of ammonium thiocynate[10].

	Experimental	Theoretical	Purity
Fe^{++}	31.02 %	31.04 %	99.93 %
$(COO)_2^{--}$	48.90 %	48.93 %	99.94 %

2.A.2 Calcination of Ferrous Oxalate :

When yellow crystalline powder of ferrous oxalate dihydrate is heated, it first loses water of crystallization, and thereafter it decomposes giving off CO_2 and CO leaving behind finely divided black Fe_3O_4.[11] If this calcination is carried out in air, then the Fe_3O_4 first formed immediately turns to reddish brown alpha Fe_2O_3 on account of easy access to O_2 at these high temperatures ($> 400^{\circ}C$).

(a) $FeC_2O_4.2H_2O \longrightarrow FeC_2O_4 + 2H_2O$

(b) $3FeC_2O_4 \longrightarrow Fe_3O_4 + 2CO_2 + 4CO$

(c) $2Fe_3O_4 + O \longrightarrow 3Fe_2O_3$

The procedure adopted to check the reaction at stage (b) was to heat ferrous oxalate in a semi-closed furnace so that the decomposition takes place virtually in an inert atmosphere of gaseous products of the reaction itself.[12] The disadvantages of this procedure are that the reaction temperature goes very high ($\backsim 700^{\circ}$- 800°C) resulting in sintering of particles. Some formation of non-magnetic α-Fe_2O_3 also takes place, as presence of some O_2 cannot be ruled out.

During the course of this investigation, it was found after trials with various atmospheres that this reaction up to stage (b) can be carried out most conveniently in a current of steam.[13] Thus finely divided yellow crystals of ferrous oxalate were converted into black oxide of iron at a temperature of 400°-450°C in a current of steam at atmospheric pressure, using apparatus shown in Fig. 2. For this operation, the hydrogen gas and the purification assembly were replaced by steam generator. Details of this set-up are described later in Section 2.B.2.

In one run about 10 grams of yellow ferrous oxalate gave 7 to 8 grams of black iron oxide in about 2.5 hours. The main product was identified by X-ray diffraction as Fe_3O_4 (magnetite), described in detail in Chapter-III.

The advantage of this process is that the chances of mutual solution or fusion of particles causing sintering

are avoided because of low temperature of decomposition. Another aspect of this procedure is that the black product of Fe_3O_4 obtained in steam is non-stoichiometric. This is discussed in detail under thermogravimetry in Chapter-III. It is found to contain extra oxygen which facilitates its further oxidation to gamma ferric oxide described below.

2.A.3 Oxidation of Fe_3O_4 to γ-Fe_2O_3 :

Fine powder of black ferrosoferric oxide obtained as described above in Section 2.A.2 was oxidised at 240°-250°C in a dynamic flow of moist air at a carefully controlled rate. Set-up described in Fig. 2 was used for the purpose of this oxidation also. The purification train and hydrogen gas supply were removed and a suction pump with a capillary flow-meter was attached at the other end. The black colour gradually turned reddish-brown in about one-two hours. This reddish-brown product was identified by X-ray diffraction as gamma ferric oxide (γ-Fe_2O_3) discussed later.

SECTION - B

FERRIC OXIDE HYDRATE PROCESS FOR THE PREPARATION OF ACICULAR GAMMA FERRIC OXIDE

2.B.1 Preparation of Acicular Ferric Oxide Hydrate :

(a) Process outline

The preparation of ferric oxide hydrate FeOOH in a definite morphology is achieved by gas-liquid-solid phase reaction involving oxidation of precipitated ferrous hydroxide by air. This is achieved in two steps.

The initial reaction involves preparation of seed nuclei by the reaction of iron salt, alkali and air. The seed formation reaction is normally conducted using excess of $FeSO_4$. This reaction may be represented by the following equations :

$$FeSO_4 + 2NaOH \longrightarrow Fe(OH)_2 + Na_2SO_4 \quad \ldots\ldots (2)$$

$$2Fe(OH)_2 + \tfrac{1}{2}O_2 \longrightarrow 2FeOOH + H_2O \quad \ldots\ldots (3)$$

As the concentration of solutions used for this step are high, very very fine precipitate results serving as nuclei for the next step.

The whole mass is then transferred to a precipitator containing dilute $FeSO_4$ solution and scrap iron. A continuous stream of air is bubbled through the heated solution. The seed particles are continuously circulated over iron in an oxidising environment where the following reactions take place.

$$2FeSO_4 + 4H_2O \longrightarrow 2Fe(OH)_2 + 2H_2SO_4 \quad \ldots\ldots (4)$$

$$2Fe(OH)_2 + \tfrac{1}{2} O_2 \longrightarrow 2FeOOH + H_2O \quad \ldots\ldots (5)$$

$$2H_2SO_4 + 2Fe + O_2 \longrightarrow 2FeSO_4 + 2H_2O \quad \ldots\ldots (6)$$

At high temperatures of 70°-$80^{\circ}C$, ferrous sulphate solution tends to hydrolyse (equation 4) to ferrous hydroxide which gets oxidised to ferric oxide hydrate (equation 5). No fresh precipitation actually occurs as the nuclei already present take up more ferric oxide hydrate thus growing in size. This further growth takes place preferentially along one axis resulting in needle-shaped crystals. The other product of hydrolysis namely sulphuric acid (equation 4) reacts with scrap iron (equation 6) regenerating ferrous sulphate. This reaction simultaneously controls the pH and does not allow it to fall below 3.2. This chain of reactions virtually means that iron gets oxidised to ferric oxide hydrate in the presence of water.

$$2Fe + H_2O + \frac{3}{2} O_2 \longrightarrow 2FeOOH \quad \ldots\ldots (7)$$

The acicular product obtained by this process is α-FeOOH.

This reaction in principle appears to be very simple. But the nature of the product is affected by a host of factors covered by a very large number of patents. Some of the salient factors involved are temperature, stirring rate, bubbling rate of air, type of scrap iron used, and the concentration of ferrous sulphate solution.

(b) Stock solutions

Reagent grade chemicals namely crystalline ferrous sulphate and sodium hydroxide were used without further purification. Scrap iron was first washed with kerosene and then with acetone to remove dirt and oil.

Ferrous sulphate solution

3 Kgs. of $FeSO_4.7H_2O$ were dissolved in 9 litres of distilled water containing about 75 ml. of concentrated sulphuric acid (density 1.8). About 100 gms. of iron metal powder was added to reduce Fe^{3+} ions if any, and the whole solution was stirred for some time. The resulting solution was filtered and analysed for exact strength by standard $KMnO_4$. The strength of the solution was adjusted to 1M strength by dilution. The pH of the solution was kept between 2.2 to 2.4.

Sodium hydroxide solution

300 gms. of NaOH flakes were dissolved in distilled water to make 5.0 litres giving approximately 1.5 N solution.

(c) Experimental :

(i) Seed material

The seed material was prepared by abruptly adding the 1.5 N sodium hydroxide stock solution to 1 M ferrous sulphate stock solution at room temperature in the ratio ranging from 0.8:1 to 0.9:1 respectively. The pH of the mixture was kept in the range of 5.5 to 5.7. The experimental set-up used (Fig. 1(a)) consisted of a simple conical flask kept on a magnetic stirrer. Air was bubbled through the solution at room temperature at the rate of 0.5 litre per minute for about one hour. The progress of oxidation of ferrous sulphate showed changes in colour from dark blue to green and finally to brownish yellow. At this stage the air flow was reduced to half (0.25 litre/min.) and maintained for about one hour more. The yellow-colloidal suspension indicates complete formation of seed material.

(ii) Seed growth

The seed material was transferred to a precipitator containing 700 ml. of 1 M ferrous sulphate stock solution and about 80 grams of scrap iron. Sufficient distilled

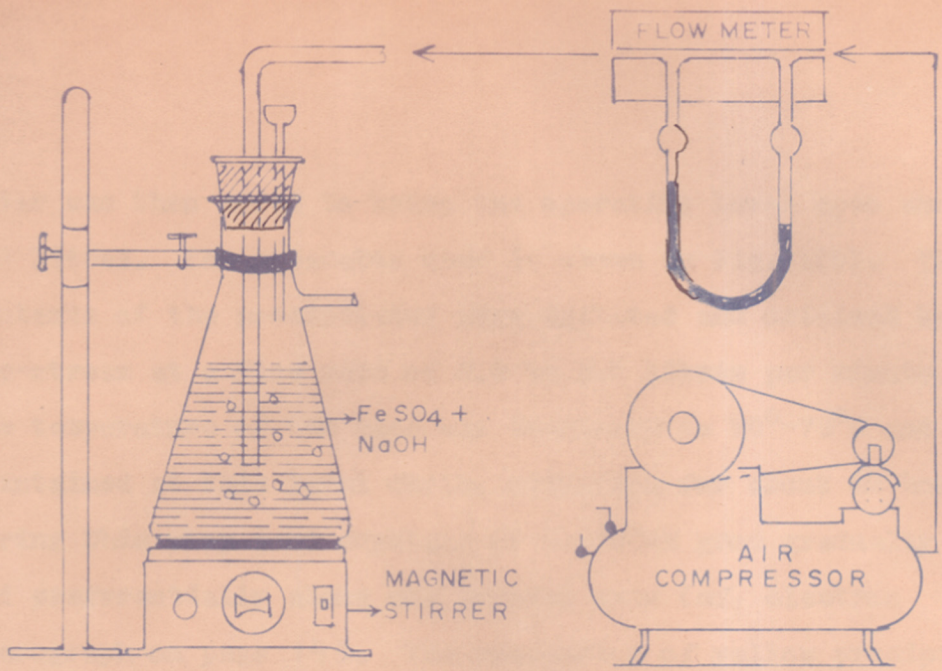

FIG. I(a) SEED PREPARATION. Stage I

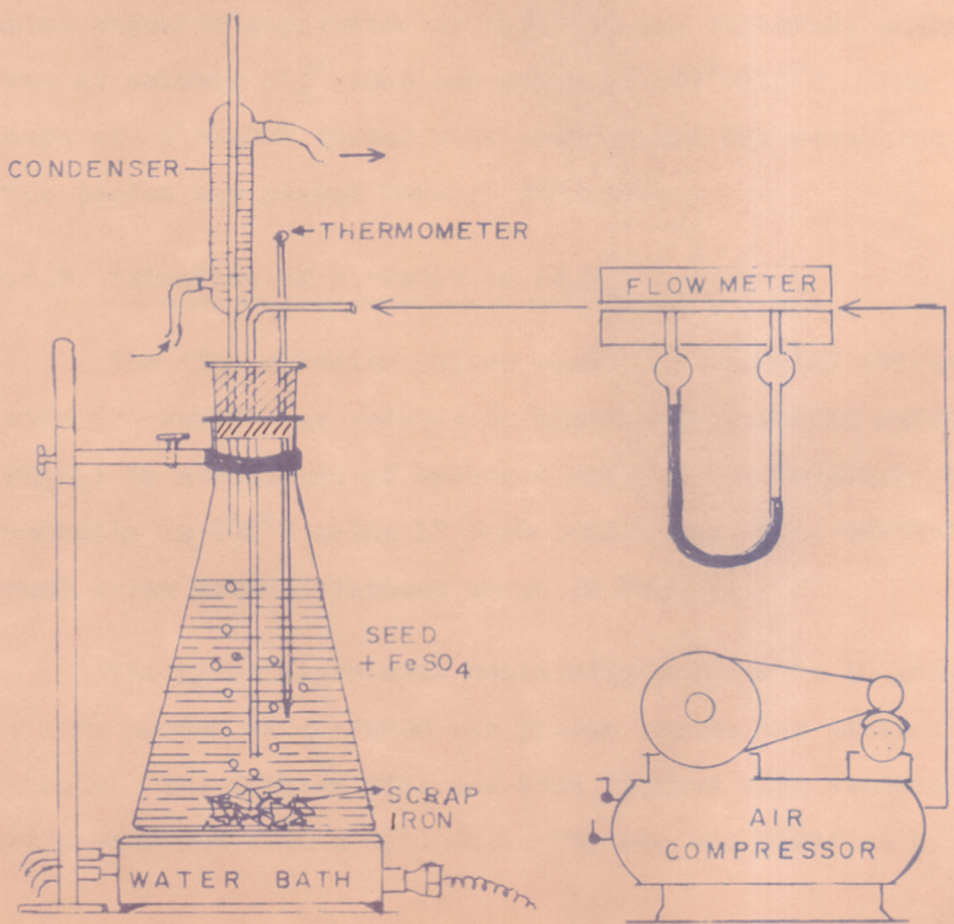

FIG. I (b) FORMATION OF α-FeOOH Stage II

water was then added to bring the operating level upto about 5.0 litres. The apparatus used is shown in Fig. 1(b). The contents of the precipitator were agitated and oxidised by air-stream at a flow rate of 2.5 to 3.0 litres per minute. The temperature of the mass was increased to 70°-75°C and maintained at this level during oxidation for about 48 hours. During this step seed crystals of α-FeOOH grow gradually and preferentially along one crystal axis (cf. electron micrograph on page 14). The suspension of yellow precipitate of α-FeOOH formed was separated by gravity settling of unreacted scrap iron, and traces of iron were removed using magnetic separation method. It was filtered, washed free of soluble SO_4^{2-} ions and dried at 100°-110°C. The lumps of α-FeOOH formed were crushed and the resulting fine powder was sieved through 250 mesh.

2.B.2 Reduction of α-FeOOH to Fe_3O_4

The fine acicular yellow powder of hydrated ferric oxide (α-FeOOH) was reduced to black ferrosoferric oxide (Fe_3O_4) in atmosphere of hydrogen raising the temperature gradually to 400°C using 18 inch long 2 inch dia. canthal wound pyrex tubular furnace shown in Fig. 2.

The pyrex glass boat containing about 5 to 10 gms. of fine powder of α-FeOOH was placed inside the tubular furnace. The furnace tube was then flushed with electrolytic hydrogen from a cylinder. The gas was purified by

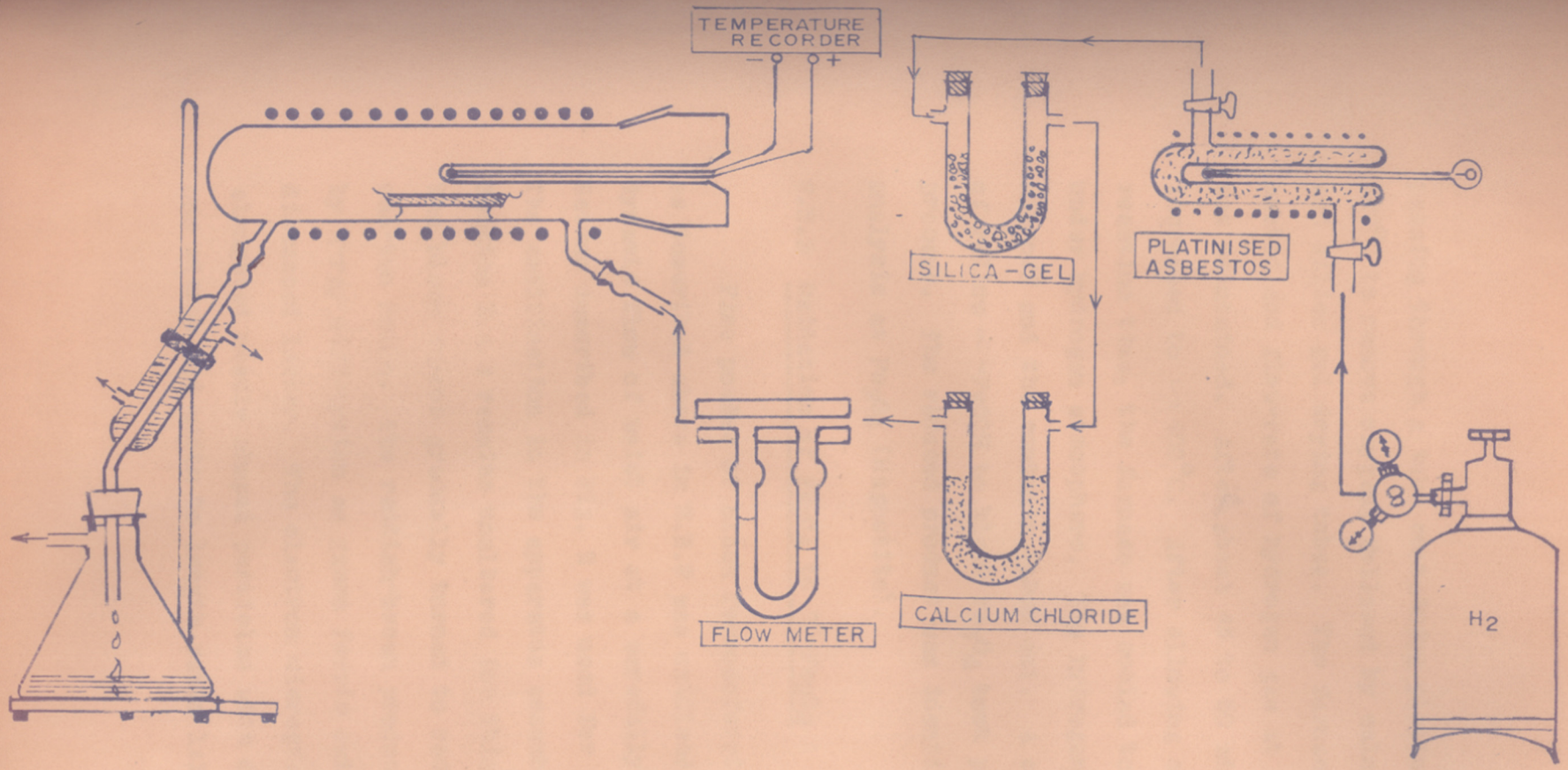

FIG. 2 : SCHEMATIC DIAGRAM OF REDUCTION PROCESS ASSEMBLY

passing through a tube containing platinised asbestos at 350°C to remove oxygen, followed by calcium chloride tower and silica gel drying tubes. The furnace was gradually heated and flow-rate of hydrogen gas at about 4-5 litres/hr. was maintained. After about 45 to 50 minutes the temperature increased to ∽ 400°C. After allowing about half an hour reaction time, the furnace was cooled to room temperature under hydrogen atmosphere. The hydrogen flow was then cut-off and the contents taken out. A complete conversion of yellow α-FeOOH to black Fe_3O_4 took place during this process. The reduced product was identified by X-ray analysis as Fe_3O_4 (Magnetite).

2.B.3 Oxidation of Fe_3O_4 to γ-Fe_2O_3 :

Fine powder of black ferrosoferric oxide obtained as described above in 2.B.2 was oxidised at 240-250°C in a dynamic flow of moist air at a carefully controlled rate. Set-up described in Fig. 2 was used for this purpose also. The modification in the apparatus assembly described in Section 2.A.3 remains unaltered for this oxidation as well. The black colour gradually turned to reddish-brown in about one-two hours. The reddish-brown product was identified by X-ray diffraction as gamma ferric oxide (γ-Fe_2O_3) discussed latter. The electron micrograph (Fig. 3) showed elongated needle shaped particles with diameters less than one micron and width to length ratio 1:10 to 1:20.

Electron micrographs of acicular alpha-FeOOH, Fe_3O_4 and gamma-Fe_2O_3 exhibiting sub-micron particle size distribution and good acicularity.

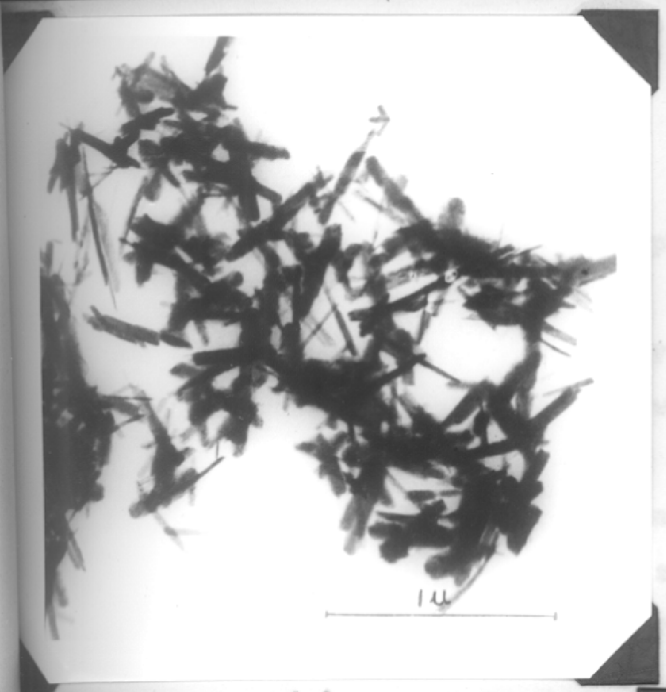

(a)

(b)

(c)

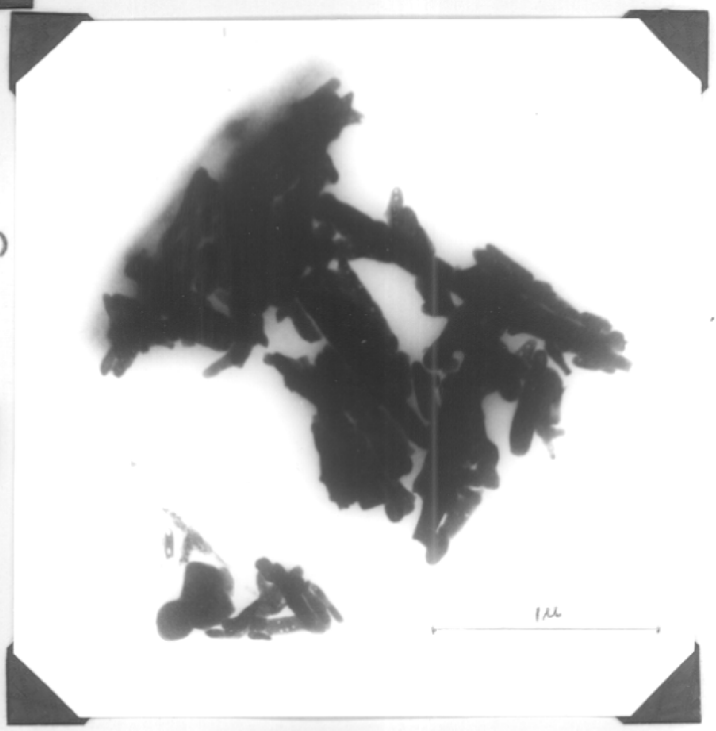

Fig. 3 : Electron micrographs at 33,480 magnifiction.
(a) alpha-FeOOH
(b) Fe_3O_4 and
(c) gamma- Fe_2O_3.

Electron micrographs at 33,480 magnification (Fig. 3) of the starting material α-FeOOH, intermediate Fe_3O_4 and the final product gamma Fe_2O_3 all revealed acicular elongated needle shape particles, which confirmed that the morphology of the original crystals is not altered through the subsequent stages of reduction (400-450°C) and reoxidation (240°-250°C). The particle size was found to be in the submicron range with width:length ratio of about 1:10 to 1:20.

CHAPTER - III : PHYSICO-CHEMICAL STUDIES

SECTION - A

THERMOGRAVIMETRIC AND DIFFERENTIAL THERMAL ANALYSES

3.A.1 Thermogravimetry :

Thermogravimetry is a technique whereby a sample is continuously weighed as it is being heated at a linear rate. The weight of the sample is plotted against time or temperature. This thermogram reveals any physico-chemical changes that are accompanied by loss or gain in weight and the temperatures at which these occur. The position of these changes in the thermogram, and the slopes of the curves are mainly influenced to some extent by two factors : (1) instrumental and (2) sample characteristics. The former includes (a) furnace heating rate, (b) recording speed, (c) furnace atmosphere, (d) geometry of the sample holder and furnace, and (e) sensitivity of recording medium. The sample characteristics include (i) amount of sample, (ii) particle size distribution, (iii) rate of removal of evolved gases, (iv) heat of reaction, (v) physical nature of the sample and (vi) thermal conductivity of the sample.

(a) TGA apparatus

The thermogravimetric unit set-up for these studies is shown in Fig. 4. It consists of the following parts :

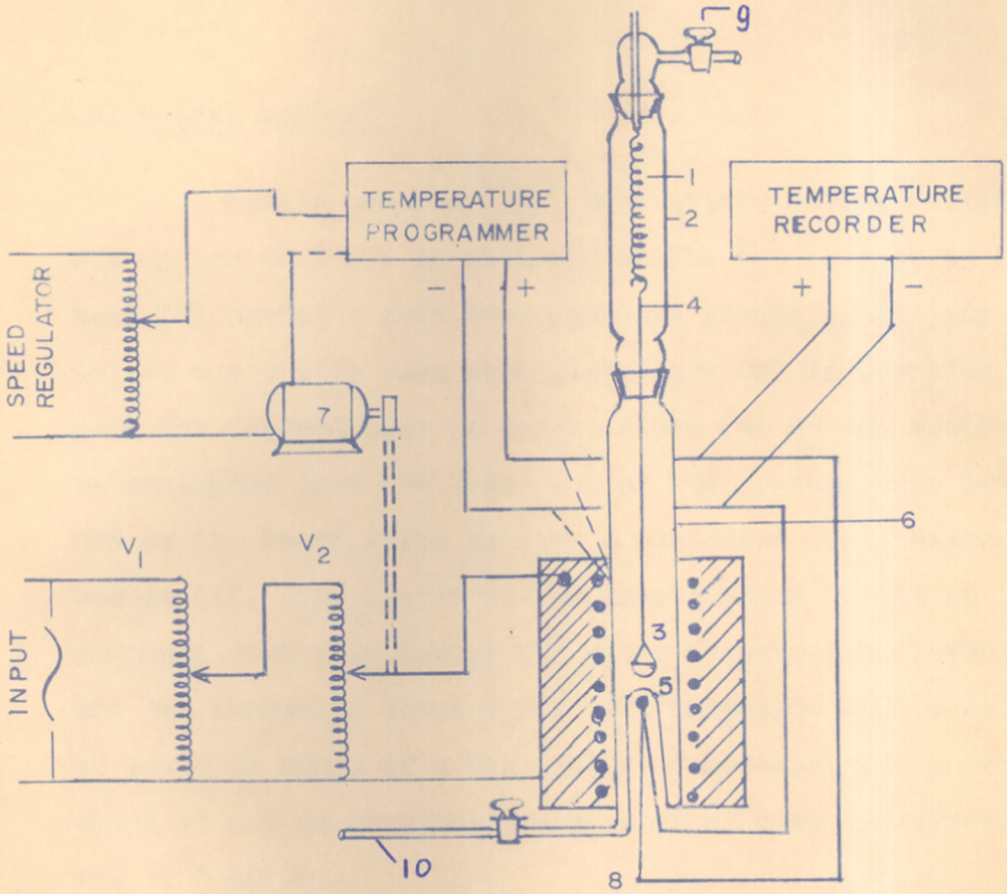

FIG : 4 :

SCHEMETIC DIAGRAM OF THERMOGRAVIMETRIC APPARATUS

(a) quartz spring, (b) fused silica furnace tube, (c) temperature programmer, and (d) temperature detecting and recording system.

(b) Quartz spring

A McBain and Bakr[14,15] type quartz spring (sensitivity 2.5 mg per cm.) (1) is enclosed at the top of a pyrex tube head (2) having a male B-40 standard ground glass joint. At the top a side tube with a stopcock (9) is provided to pass the desired gas. A quartz fibre (4) in two sections is suspended from the lower end of the spring. The lower end of the lower fibre carries a suspended small aluminium bucket (3). The length of the quartz fibre (4) is so arranged that when loaded the space between the thermowell (5) and the bucket is about 4 mm. The extension of the spring is noted by means of a travelling microscope with a least count of 0.1 mm enabling measurement of mass differences as low as 0.25 mg.

(c) Furnace tube

The lower part of the balance consists of a fused silica tube (6) wound with nichrome tape covered with thick asbestos rope insulation. It has a B-40 female standard ground joint at the top to fit the quartz spring head assembly. It has a thermowell (5) and a side exit tube (10).

(d) Temperature programmer

The input E.M.F. fed to the furnace is increased gradually by means of a dimmerstat (variac V_1) coupled to an ordinary variable speed motor (7) which controls the rate of heating. The highest temperature attained by the system is controlled by providing a range selector variac V_2 which controls the total voltage present on variac V_1. The rate of heating obtained in any range was found to be almost linear.

(e) Temperature recorder

A chromell-alumel thermocouple (8) was used for measuring the temperature of the furnace which was recorded continuously on an Elliot-electronic strip-chart recorder. The recorder has an inbuilt standard cell for automatic standardisation.

(f) Sample preparation

All the samples were ground to 250 mesh in an agate-pestel and mortor. Tight packing of the sample leads to non-uniformity of temperature in the sample.[16] Therefore, a loose packing of the material which affords easier diffusion of gaseous products from the material was used in the present case.

3.A.2 Differential Thermal Analysis :

Differential thermal analysis is a technique by which enthalpy changes associated with physical and chemical phenomena are recorded as a function of temperature. These thermal effects are caused by decomposition and phase transformations in the sample. The sensitivity of this technique depends upon the use of a differential thermocouple which records the difference in temperature of the sample and that of an inert material generally alumina. Thus height of the peak and area under the curve corresponding to any enthalpy change, is increased appreciably, which depends upon the rate of that phenomenon.

The number, shapes and positions of the various endothermic and exothermic peaks with respect to the furnace temperature can be used as a means for qualitative identification as well as quantitative estimation of the substance under investigation.

The height of the peaks and the peak area are influenced to some extent by factors of two principle types, namely (a) instrumental and (b) sample characteristics. The latter includes (i) particle size distribution, (ii) thermal conductivity, (iii) heat capacity, (iv) packing density, (v) swelling or shrinkage of sample, (vi) amount of sample, (vii) degree of crystallinity, rate of removal

of evolved gaseous products, heat of reaction etc. The instrumental factors include among others (1) heating rate, (2) recording speed, (3) furnace atmosphere and (4) geometry of the sample-holder and the furnace.

(a) DTA instrument

An automatic derivatograph type OD/102 MOM-Budapest (Hungary) was used for these studies.

Preliminary runs with calcium oxalate monohydrate were carried out to check the reproducibility of the results. The peak temperatures for both dehydration and decomposition were found to be reproducible within $\pm$ 2°C and these agreed with literature data.

(b) Application of DTA

In recent years, the technique of DTA has been employed as a tool to provide supporting evidence on the structure of iron oxides of technical importance. Lodding and Hammell[17] used this technique to characterise iron oxides mixed with gibbsite $Al(OH)_3$. Simon et al.[18] examined the calcination of magnetite to gamma ferric oxide. Inouye[19] studied the mechanism of growth of pure α-FeOOH and copper dopped α-FeOOH by DTA. Erdey[20] applied the DTA technique to determine the presence of α-Fe_2O_3 in gamma ferric oxide. Arora et al.[21] have used the DTA

technique to elucidate the conversion efficiency of ferric oxide alone and ferric oxide-chromium oxide mixed catalysts. Mukherjee and Roy[22] studied by this technique the role of iron oxide in the co-precipitated binary Al_2O_3-Fe_2O_3 system. Sastri et al.[23] followed by means of DTA the reduction of ferric oxide samples prepared in different ways.

3.A.3 TGA and DTA Studies of Ferrous Oxalate Dihydrate Decomposition :

Typical TGA curves of $FeC_2O_4.2H_2O$ obtained in atmospheres of hydrogen, nitrogen and oxygen and of an anhydrous sample in oxygen are shown in Fig. 5. This figure also includes one DTA curve in air. Heating rate in TGA studies was 4°/min., and 10°/min. in DTA studies.

It may be worth recording that the flow rate of gas in the range of 0.01 to 2.5 litres per minute, and small changes in pressure in the reaction chamber (750-770 mm Hg.) did not have any appreciable effect on the reaction temperature of a sample. However, the purity of the gas was found to be extremely important. Presence of very very small quantity of oxygen in nitrogen at first gave misleading result showing decomposition temperature of ferrous oxalate as low as 210°C-the same as in air- instead of about 350°C found latter on in purified nitrogen. Hence, all gases used in these experiments were carefully purified. Hydrogen gas was passed through a tube containing platinised

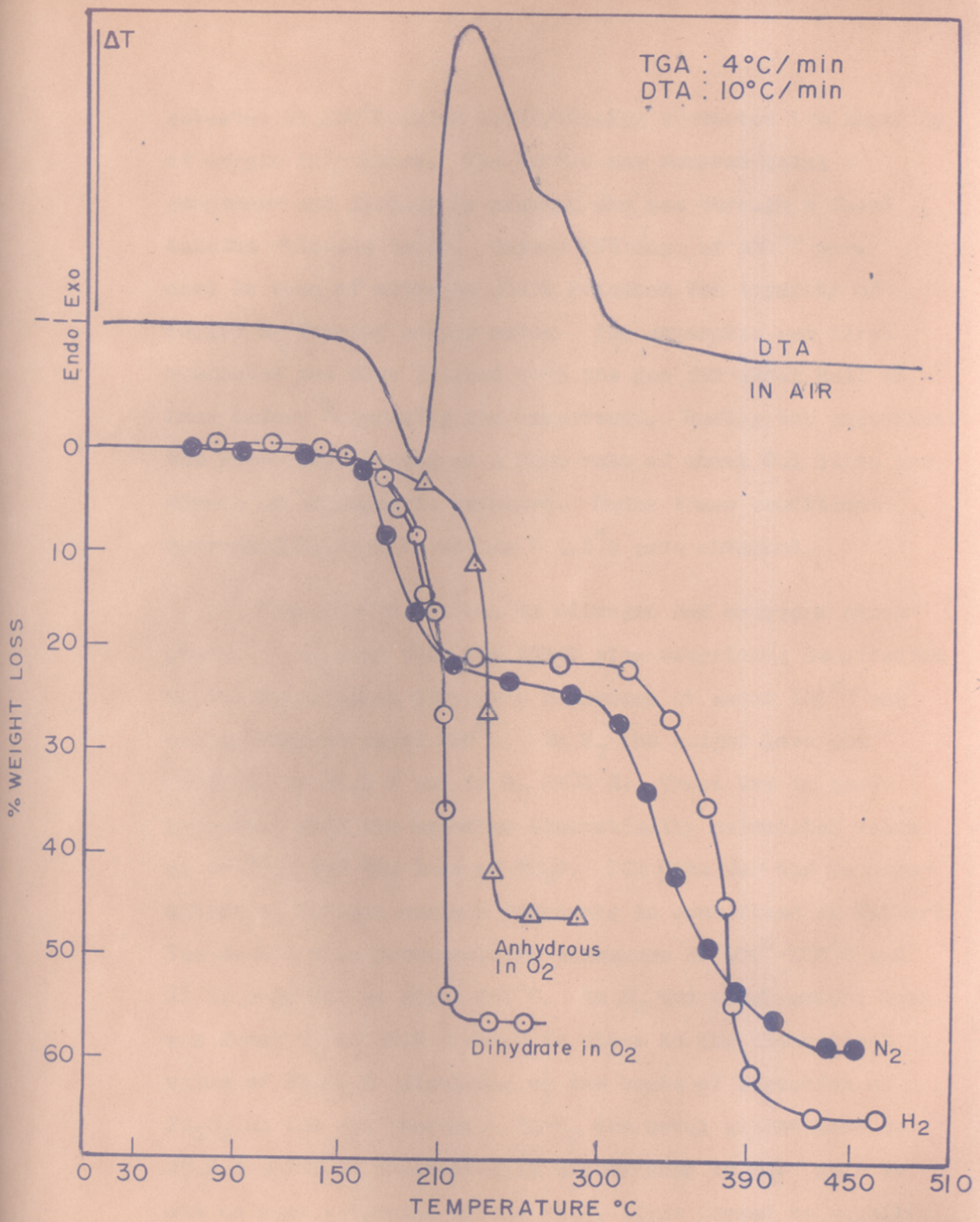

FIG: 5 : TGA AND DTA OF FERROUS OXALATE DIHYDRATE

asbestos at 350°C which catalytically converted the impurity of oxygen into water. The latter was removed using a condenser and further by passing the gas through a fused calcium chloride tower. Copper fillings at 350°C were used in case of nitrogen which retained the impurity of oxygen by forming copper oxide. The apparatus was first evacuated and then flushed with the gas for about half an hour before commencing the experiment. During the experiment the gases were passed at a flow rate of about 0.1 litre per minute at atmospheric pressure. Under these conditions reproducible results within ± 1.5°C were obtained.

From the TGA curves in nitrogen and hydrogen atmosphere, it is seen that the first step comprising dehydration of ferrous oxalate dihydrate commences at about 150°C and is complete at about 200°C. In N_2 the weight loss was found to be 20.5 % and in H_2 19.5 %. These are in good agreement with the expected theoretically calculated value of 20.03 % for the loss of $2H_2O$. TGA data for the decomposition of ferrous oxalate dihydrate is summarised in Table-1. The second step decomposition commences at 300°-320°C and it is complete at about 420°C. In N_2 the total weight loss was found to be 58.0 % which is close to the theoretical value of 57.04 % calculated on the basis of formation of Fe_3O_4 as the end product. In H_2 the total weight loss is 65.5 % which is substantially higher than in N_2. This is due to some reduction of the Fe_3O_4 first formed to metallic iron.

TABLE - 1

TGA data for the decomposition of Ferrous Oxalate Dihydrate

Gas atmosphere	I step (dehydration)			II step (decomposition)			Total % weight loss
	Temperature(^{o}C)		% weight loss	Temperature(^{o}C)		% weight loss	
	Onset	Completion		Onset	Completion		
Nitrogen	150	210	20.5	300	400	37.5	58.0
Hydrogen	150	208	19.5	320	420	46.0	65.5
Oxygen (dihydrate sample)	140	212	56.5	-	-	-	56.5
Oxygen (anhydrous sample)	160	230	46.0	-	-	-	46.0

In oxygen (as well as in commercial N_2) both the steps of dehydration and decomposition get merged into a single step. Both hydrated as well as anhydrous sample showed the same phenomenon. This indicates that in ferrous oxalate some slight tendency to decompose manifests itself even at about 200°C. This decomposition is further helped in oxygen when the liberated carbon monoxide is immediately oxidised to carbon dioxide. This reaction being exothermic, the liberated local heat leads to completion of decomposition. It may be noted here that the decomposition step in the case of anhydrous ferrous oxalate is somewhat higher (160°-230°C) than in the hydrated form (140°-212°C). This indicates that in the hydrated form the liberation of water molecules from the crystals aids the liberation of CO as well as for the above explained decomposition to take place at a lower temperature.

This one step decomposition of ferrous oxalate was also revealed in the DTA studies in air coinciding with the TGA curve. The dehydration and decomposition step starts as an endothermic peak but it soon changes into an exothermic peak due to the exothermic oxidation of liberated CO to CO_2. Close examination of the exothermic peak reveals a distinct shoulder in the decreasing phase of the reaction. This clearly indicates that there must be two reactions proceeding side by side. This second exothermic part

appears to be due to the oxidation of Fe_3O_4 to Fe_2O_3.

The mechanism of decomposition of ferrous oxalate dihydrate is thus indicated to be :

$$FeC_2O_4.2H_2O \xrightarrow{150^\circ-200^\circ} FeC_2O_4 + 2H_2O \ (I) \quad ..... \quad (8)$$

$$3FeC_2O_4 \xrightarrow[\text{inert atmosphere}]{300^\circ-420^\circ} Fe_3O_4 + 4CO + 2CO_2 \ (II) \quad ..... \quad (9)$$

According to this mechanism the weight loss in the decomposition of ferrous oxalate dihydrate should be 57.04 %. Gunther and co-workers[24] have proposed that the decomposition takes the following course.

$$FeC_2O_4 \longrightarrow FeO + CO + CO_2 \quad ..... \quad (10)$$

$$4FeO \longrightarrow Fe_3O_4 + Fe \quad ..... \quad (11)$$

According to them the first product is FeO which further disproportionates into Fe_3O_4 and Fe. This mechanism would require a total weight loss of 60.07 %. Our observed value of 58.0 % is much nearer the mechanism shown by equations (8) and (9) than the equations (10) and (11). In fact Macklen[25] also observed total weight loss which was appreciably lower than their theoretical value of 60.07 %. We are thus inclined to believe that decomposition

of ferrous oxalate dihydrate predominantly results in the formation of Fe_3O_4, although formation of other oxides cannot be ruled out.

The mechanism of decomposition in H_2 would be the same upto step II shown in equations (8) and (9), and then further reduction to Fe takes place.

$$Fe_3O_4 + 4H_2 \longrightarrow 3Fe + 4H_2O \quad \ldots\ldots (12)$$

Similarly in O_2 dehydration and decomposition mechanisms are the same but Fe_3O_4 is simultaneously oxidised to Fe_2O_3 which is thus obtained as the only end product.

$$2Fe_3O_4 + O \longrightarrow 3Fe_2O_3 \quad \ldots\ldots (13)$$

In view of our observation that ferrous oxalate dihydrate decomposes to Fe_3O_4 in the second step at 300°-400°C, it was considered reasonable to try the large scale decomposition in a current of steam. This approach gave very encouraging results in that the decomposition proceeded smoothly at this low temperature (450°C), and the Fe_3O_4 product obtained was of submicron size showing no sintering effect at this low temperature. Use of steam has the additional advantage that moisture is known to play a vital role in stabilizing the structure of Fe_3O_4.

3.A.4 TGA and DTA Studies of Alpha Ferric Oxide Hydrate Decomposition :

Typical TGA curves of ferric oxide hydrate in air and in hydrogen are shown in Fig. 6. The DTA curve obtained in air is also shown in this diagram. The weight loss in air due to dehydration was observed to be 10.3 % which agrees with the theoretical value calculated according to the following equation.

$$2FeOOH = Fe_2O_3 + H_2O \quad \ldots\ldots (14)$$

The dehydration appears to commence at about 175°C and is complete at about 300°C. TGA data for the decomposition of alpha FeOOH is summarised in Table-2.

It was, however, noticed that the final weight of Fe_2O_3 product remains constant for a very short interval. A slow loss of weight starts again at about 350°C and was still going on till 600°C upto which the experiment could be carried out with an aluminium bucket. This slow reaction appears to indicate the loss of oxygen forming Fe_3O_4.

$$3Fe_2O_3 \longrightarrow 2Fe_3O_4 + O \quad \ldots\ldots (15)$$

This agrees with the fact that the curve tends to indicate the final total weight loss of about 13 % corresponding to

TABLE - 2

TGA data for the decomposition of Alpha Ferric Oxide Hydrate

Gas atmosphere	I Step			II Step			Total % weight loss
	Temperature (°C)		% weight loss	Temperature (°C)		% Weight loss	
	Onset	Completion		Onset	Completion		
air	175	300	10.31	-	-	-	-
hydrogen	225	360	13.1	390	490	24.2	37.3

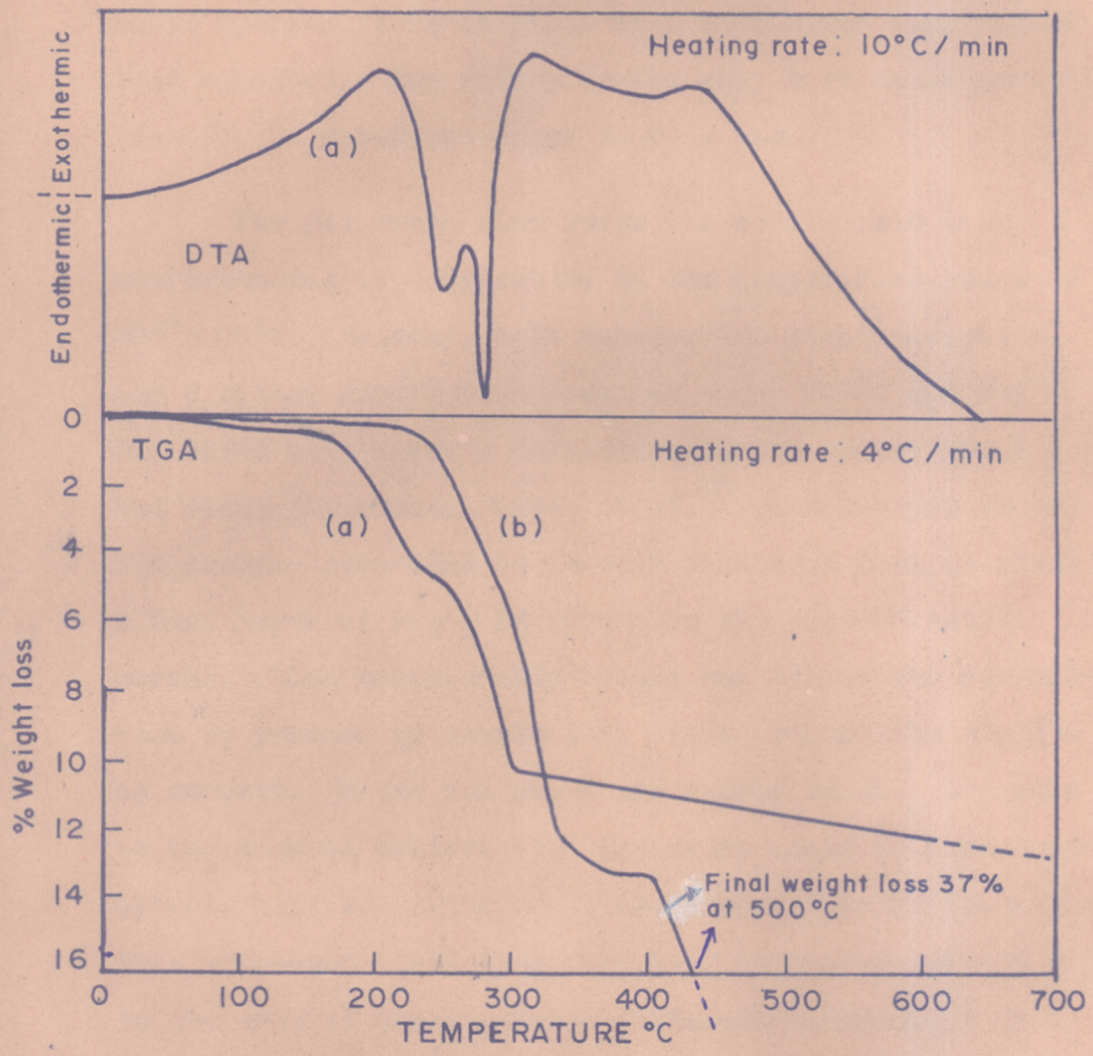

FIG. 6. TGA AND DTA OF ALPHA FERRIC OXIDE HYDRATE

(a) In air (b) In hydrogen

the formation of Fe_3O_4. This conversion of Fe_2O_3 to Fe_3O_4 is already known, but in the case of dehydration of ferric oxide hydrate it takes place at a much lower temperature than expected. The reason is the very very small particle size in the submicron range in this case.

The DTA curve also shows the endothermic step corresponding to dehydration in the temperature range of 200°-300°C. However, this dehydration step consists of two distinct endothermic peaks at about 250°C and 275°C. TGA curve also shows a deflection in the middle showing a two stage phenomenon. Derie et al.[26] also noticed these two peaks. According to them it indicates that at first a hard layer of Fe_2O_3 is formed on the core of FeOOH crystal which subsequently breaks and allows the dehydration to proceed to completion. This explanation may not be correct. These two steps are nearly equal. It would be too much to believe that the crust would be formed upto exactly half the extent. We are inclined to believe that this phenomenon indicates that half the number of -OH groups in the crystal have somewhat different environment than the other half. This may require further investigation.

In hydrogen atmosphere the weight loss in the first step is about 13 %. This agrees with the theoretical value

calculated on the basis of formation of Fe_3O_4.

$$3FeOOH + H \longrightarrow Fe_3O_4 + 2H_2O \quad \ldots\ldots \quad (16)$$

From our TGA curve in hydrogen it thus appears that alpha ferric oxide hydrate in hydrogen is directly converted to Fe_3O_4 in one single step (small deflection is due to different environment of about half the number of -OH groups in the crystal discussed above). There is no evidence to show the formation of Fe_2O_3 first which is reduced subsequently to Fe_3O_4 as is generally believed.

In hydrogen, it appears that Fe_3O_4 formed is stable in a very narrow range of temperature. When the temperature rises above 400°C, it gets further reduced to metallic Fe which is complete by about 490°C.

$$Fe_3O_4 + 4H_2 \longrightarrow 3Fe + 4H_2O \quad \ldots\ldots \quad (17)$$

The reduction temperature observed here is very much lower than normally expected, which is again due to the submicron particle size of the crystallites. This observation is of some importance in the preparation of gamma ferric oxide.

It may be worth pointing out that the first step in hydrogen commences at an appreciably higher temperature (225°C) than in air (175°C). This is rather unexpected. It may have some basic significance, or it may be due to some thermal lag as hydrogen is a poorer conductor of heat than air.

We are inclined to believe in the latter cause.

3.A.5 TGA studies of Fe_3O_4 Oxidation :

As already reported above, Fe_3O_4 was prepared by two methods: (a) by heating α-FeOOH in H_2 and (b) by heating $FeC_2O_4.2H_2O$ in steam. Thermograms of both these samples in air at a heating rate of $4^{\circ}C$/min. are shown in Fig. 7. These thermograms show that oxidation of both these varieties starts almost immediately at such a low temperature as $60^{\circ}C$, and is complete by about 250°-$280^{\circ}C$. This indicates that Fe_3O_4 obtained by both these techniques is in a very reactive form which appears to be due to the formation of fine particles of less than one micron.

$$2Fe_3O_4 + O \longrightarrow 3Fe_2O_3 \text{ (gamma)} \qquad \ldots\ldots \quad (18)$$

According to the above equation (18), the theoretical gain in weight of Fe_3O_4 should be 3.46 %. The experimental value of percentage gain in weight is appreciably less than this calculated value. It is 2.71 % in case of sample (a) and 2.33 % for the sample (b). This indicates that both these varieties of Fe_3O_4 are non-stoichiometric. This is because both these varieties are in a very reactive form, and as such they take up oxygen from the air during their preparation. From these studies it appears that Fe_3O_4 indicated as (b) in Fig. 7 obtained by heating ferrous oxalate in steam is relatively more reactive and its

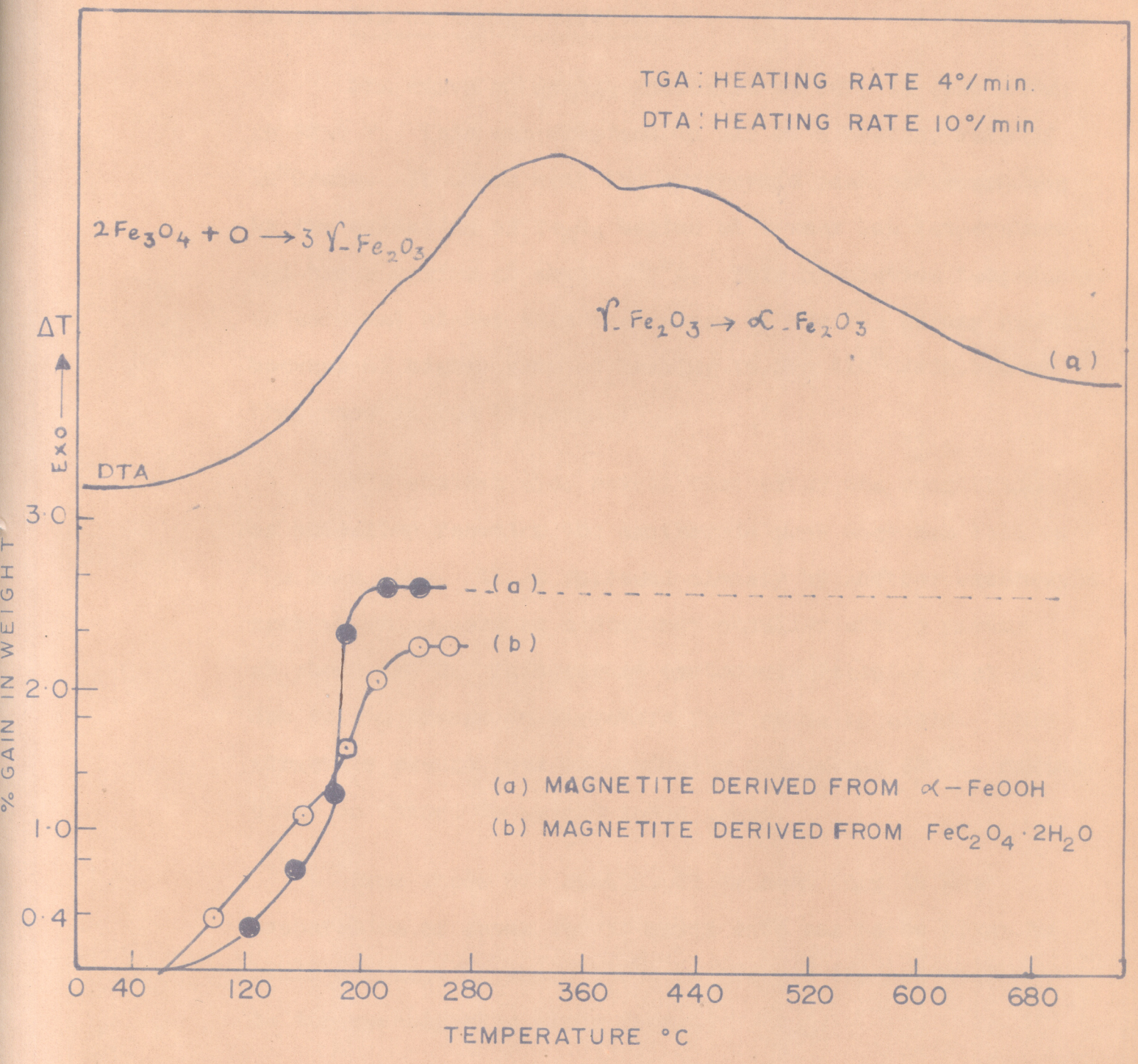

FIG: 7: TGA AND DTA OF Fe_3O_4 (MAGNETITE) IN AIR

composition deviates from stoichiometry to a greater extent.

3.A.6 DTA of Fe_3O_4 Oxidation :

DTA curve of Fe_3O_4, indicated as (a), is also shown in Fig. 7. This was obtained in air at a heating rate of $10^{\circ}C$/min. It shows that the exothermic peak corresponding to the oxidation of Fe_3O_4 begins at a very low temperature and has a maxima at about $300^{\circ}C$. This completion temperature is somewhat higher than that shown by the TGA curves probably because of higher rate of heating in DTA ($10^{\circ}C$/min.) than that used in TGA ($4^{\circ}C$/min.)

DTA studies also reveal that after the completion of oxidation reaction the exothermic peak does not fall to the base line. It is followed closely by another exothermic peak which appears as a distinct shoulder with a maxima at about $450^{\circ}C$. This second exothermic reaction must be due to the change in structure from gamma to alpha. This structure change goes on gradually upto about $650^{\circ}C$, during which no change in weight takes place.

From these DTA studies it is seen that in the preparation of gamma ferric oxide care has to be taken to avoid overheating above $300^{\circ}C$ to prevent its conversion to the non-magnetic alpha form.

It was also observed that oxidation of dry Fe_3O_4 in dry air was very sluggish. It took about 24 hours to

complete at 300°C and this prolonged treatment resulted in the formation of alpha Fe_2O_3 as the predominant product. On the other hand moist Fe_3O_4 in moist air readily oxidised at 250°C in about 6 hours giving gamma Fe_2O_3 as the only product.[27,28]

SECTION - B

MAGNETIC PROPERTIES

The normal ferric oxide in the alpha form is non-magnetic. However, the gamma form of ferric oxide is ferromagnetic, on account of which it has many applications especially in the coating of magnetic recording tapes. The magnetic properties of interest are (a) saturation magnetization σ_s, (b) remanence (Br), and (c) coercivity (H_c).

3.B.1 Saturation Magnetization :

The saturation magnetization σ_s (saturation moment per gram) was measured by Ponderometric method.[29] In this technique the specimen is allowed to oscillate at the tip of a horizontal pendulum in an inhomogeneous magnetic field perpendicular to the direction of oscillation. The square of the period of oscillation is inversely proportional to the magnetization of the sample. Thus saturation magnetization can be obtained from the following relationship.

$$\sigma_s = \frac{C}{W}\left(\frac{1}{T^2} - \frac{1}{T_o^2}\right) \qquad \ldots\ldots (19)$$

where C = constant of proportionality

$= 4\pi^2 M/a$

W = Weight of the sample

T = Periodic time when the field is on.

T_o = Periodic time when the field is off.

M = Weight of the pendulum.

a = Cross sectional area of the pendulum.

A weighed quantity of the test sample under investigation was put in a silica capsule, which was inserted on to one end of a long thin silica rod. This silica rod was suspended perpendicular to the direction of the magnetic field by four strings in two pairs, each pair forming an angle of about 60°. At resting position, the material in silica capsule was exactly at the centre of the pole gap of an electromagnet. The silica rod alongwith the sample was allowed to oscillate at right angles to the field. The periods of oscillation with and without the field were determined.

Saturation magnetization of Fe_3O_4 and γ-Fe_2O_3 samples were determined and are given in Table-3. The values are expressed in C.G.S. units (gauss/cm^3/gm.). The constant C was determined by calibrating with pure nickel metal.

It is seen from Table-3 that the saturation magnetization of Fe_3O_4 prepared from α-FeOOH is somewhat higher (90) than that of Fe_3O_4 prepared from ferrous oxalate (87.5).

TABLE - 3

Room temperature saturation magnetization of Fe_3O_4 heated to various temperatures in air for the formation of γ-Fe_2O_3

Fe_3O_4 from $FeC_2O_4 \cdot 2H_2O$			Fe_3O_4 from α-FeOOH		
Temperature of formation (°C)	% gain in weight	σ_s (C.G.S.)	Temperature of formation (°C)	% gain in weight	σ_s (C.G.S.)
		Fe_3O_4			Fe_3O_4
30	-	87.5	30	-	90.0
155	0.25	85.6	155	0.78	88.2
165	1.06	84.2	165	1.00	87.0
185	1.60	83.1	185	2.00	84.1
205	2.00	82.00	205	2.3	82.0
220	2.33	78.0	220	2.7	80.0
250+	2.33	74.0	250+	2.71	76.2
250‡	2.33	73.9	250‡	2.71	76.03
250‡‡	2.33	71.0	250‡‡	2.71	76.0
		γ-Fe_2O_3			γ-Fe_2O_3

\+ Sample heated upto 250°C

‡ Sample heated at 250°C for 1/2 hour

‡‡ Sample heated at 250°C for 1 hour

Similarly the γ-Fe_2O_3 prepared from α-FeOOH has a higher saturation magnetization (76.2) than that of γ-Fe_2O_3 prepared from ferrous oxalate (74.0). It is also seen that the value of σ_s of the latter falls appreciably when heating is prolonged, while that of former is affected slightly. These magnetic studies also reveal that while thermogravimetric gain in weight indicates the completion of reaction at 220°C, the structure seems to stabilize magnetically at 250°C.

3.B.2 Measurement of Remanence and Coercivity :

Magnetization of a ferromagnetic material is known to exhibit the phenomenon of hysteresis. When an increasing magnetic field H is applied, the induction (B) gradually increases to a maximum value called saturation. Now when the applied field (H) is gradually decreased, the induction (B) does not follow the same curve as obtained during magnetization. Induction appears to lag behind, with the result that when the magnetizing field (H) is reduced back to zero, there still remains some induction in the sample called remanence (Br). This is of importance in the use of gamma ferric oxide in recording tapes, as it represents the useful magnetic retention of the material. For a fairly good material remanence value should be about 1000 C.G.S. units.

If the applied magnetic field is further increased gradually in the reverse direction, then the remanent induction (Br) gradually decreases till it becomes zero at a certain value of the magnetic field (H_c) applied in the reverse direction. This value of H_c is called coercivity, which is another useful property as it provides a measure of the force to magnetise and demagnetise the material. For recording tapes it should not be very low otherwise the tape-recordings would get demagnetised easily. The coercivity should not be too high otherwise it would be difficult to record and equally difficult to erase the recording for fresh work. For magnetic tape recording materials a value of about 250-400 Oersteds of coercivity is considered best for this purpose.

Both remanence and coercivity can be determined from the hysteresis loop. The induction (B) is measured by means of a calibrated ballistic galvanometer. The field intensity of the electromagnet is measured at various applied e.m.f. (and current 'I' in the coils) by means of standard search-coil. The studies were conducted on gamma ferric oxide obtained from (a) ferrous oxalate and (b) from alpha ferric oxide hydrate. The materials were prepared in a pellet form of 1 cm. dia. and 1 cm. height at a pressure of 5000 lbs./cm^2, using 2% polyvinyl acetate in acetone as the binder. Typical hysteresis curves obtained

TABLE - 4

Magnetic properties of gamma ferric oxide obtained from (a) Ferrous Oxalate and (b) Ferric Oxide Hydrate

	Sample	Oxidising temperature (^{o}C)	Time (hours)	H_c (Oersted)	B_r (Gauss)
(a)	Fe_3O_4	-	-	110	850
	Heating stage-1	160	1	172	900
	Heating stage-2	200	2	188	900
	Heating stage-3 (γ-Fe_2O_3)	240	6	200	900
(b)	Fe_3O_4	-	-	115	950
	Heating stage-1	160	1	194	1000
	Heating stage-2	200	2	218	1100
	Heating stage-3 (γ-Fe_2O_3)	240	6	250	1100

are shown in Fig. 8. It is seen that γ-Fe_2O_3 obtained from alpha ferric oxide hydrate has higher remanence and coercivity than gamma ferric oxide obtained from ferrous oxalate. The squareness of the hysteresis curve in these samples is less than desired, but still the squareness also is better in the sample from ferric oxide hydrate than in the sample obtained from ferrous oxalate.

Values of coercivity (H_c) and remanence (Br), for Fe_3O_4 samples obtained from (a) ferrous oxalate and (b) from ferric oxide hydrate when heated to increasing temperatures to increasing time are shown in Table-4 for both varieties. It is evident that gamma ferric oxide from alpha ferric oxide hydrate is superior to the one obtained from ferrous oxalate. These results once again show that conversion of Fe_3O_4 to stable γ-Fe_2O_3 is complete by about 240°-250°C.

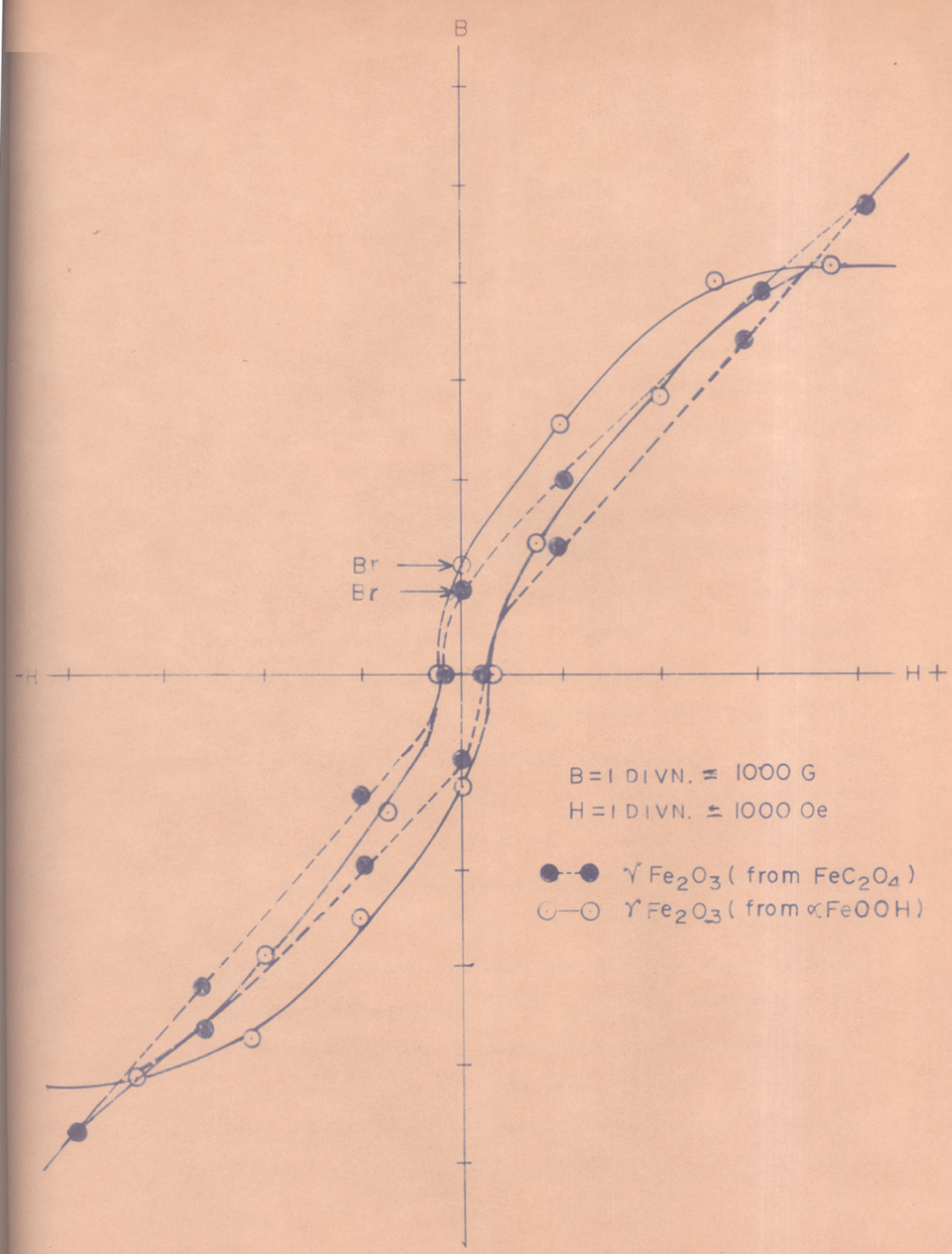

FIG: 8 : B-H CURVE FOR $\gamma - Fe_2O_3$

SECTION - C

X-RAY DIFFRACTION

Structure studies in any system are largely helped by the use of X-rays. Powder diffraction patterns of ferric oxide hydrate, ferrous oxalate dihydrate, gamma ferric oxide and the intermediate Fe_3O_4 were taken with a Debye-Scherrer camera of 11.2 cm. diameter on Philips PW 1010 X-ray unit. All the samples were ground to 250 mesh in agate-pestel and mortor before X-ray diffraction studies. The exposure time was three hours in all cases. Fe-K_α and Co-K_α radiations were used. Angles of diffraction (θ) were calculated using the geometrical dimensions. The d-values of inter-planar spacings were obtained from standard tables for Fe-K_α and Co-K_α radiation. These values of lattice spacings (d $\mathring{A}$) for all the samples are summarised in Table-5. A few typical powder diffraction patterns are shown in Fig.9. The data for lattice spacings and corresponding observed intensities with standard ASTM values for the above compounds are given in Table-5. The observed values are found to be in good agreement with the standard data reported in the ASTM cards, which confirms their identity and purity as no lines for the possible interfering compounds are present.

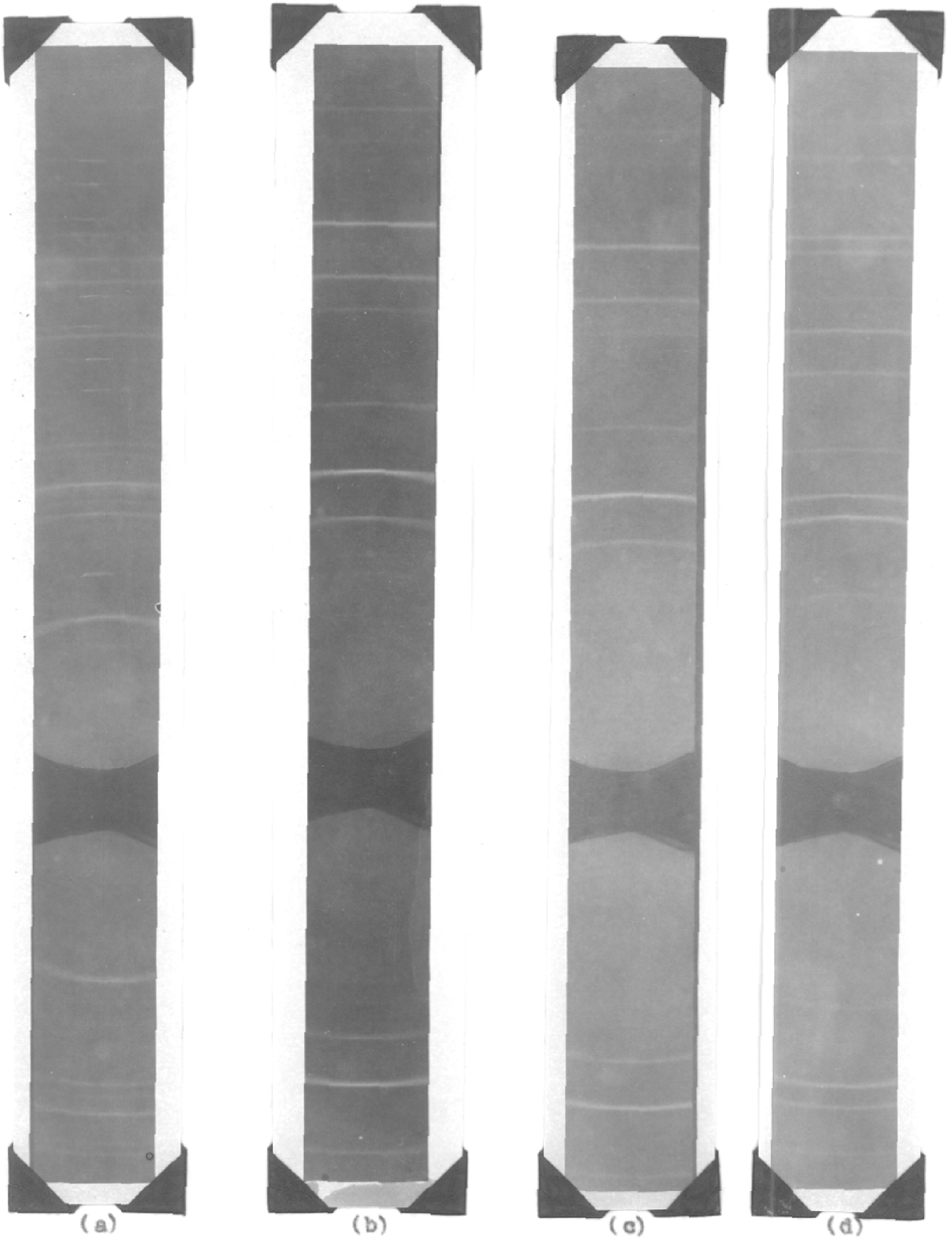

Figure - 9 : X-ray diffraction patterns.
(a) α-FeOOH, (b) Fe_3O_4
(c) γ-Fe_2O_3 (d) α-Fe_2O_3

TABLE - 5

Lattice spacings for α-FeOOH, Fe_3O_4, γ-Fe_2O_3 (Fe-K_α), and $FeC_2O_4.2H_2O$(Co-K_α)

α-FeOOH			Fe_3O_4			γ-Fe_2O_3			α-Fe_2O_3			$FeC_2O_4.2H_2O$		
$I_{obs.}$	d Å		$I_{obs.}$	d Å		$I_{obs.}$	d Å		$I_{obs.}$	d Å		$I_{obs.}$	d Å	
	obs.	ASTM 3-0249		obs.	ASTM 1-1111		obs.	ASTM 4-0755		obs.	ASTM 5-0637 3-0800		obs.	ASTM 1-0292
S	4.90	4.97	VVW	4.76	4.85	VVW	4.78	4.80	VVW	3.62	-	VS	4.90	4.75
VS	4.13	4.18	W	2.96	2.97	W	2.93	2.95	VS	2.70	2.71	W	3.90	3.83
S	2.68	2.69	VS	2.52	2.53	VS	2.51	2.52	M	2.51	2.52	W	3.10	2.98
M	2.57	2.58	W	2.09	2.10	W	2.07	2.08	W	2.2	-	W	2.60	2.61
S	2.43	2.44	VW	1.70	1.71	VVW	1.70	1.70	M	1.83	-	VVW	2.25	2.23
S	2.24	2.25	S	1.60	1.61	W	1.62	1.61	S	1.68	1.69	VVW	2.11	2.09
S	2.18	2.18	S	1.48	1.48	S	1.48	1.48	W	1.50	-	VVW	1.82	1.81
M	1.92	1.92	VW	1.27	1.28	VVW	1.32	1.32	W	1.45	-			
M	1.80	1.80				VVW	1.27	1.27						
S	1.71	1.70												
M	1.69	1.69												
M	1.60	1.60												
S	1.56	1.56												
S	1.50	1.51												
S	1.45	1.45												
M	1.42	1.42												
VVW	1.36	1.35												

VS = very strong
S = strong
M = medium
W = Weak
VW = very weak
VVW = very very weak

It will be observed from Table-5 that the structures of Fe_3O_4 and γ-Fe_2O_3 are almost identical. This is the reason why gamma ferric oxide can be obtained only through Fe_3O_4.

REFERENCES

REFERENCES

1. L.A. Welo and O. Baudisch, Phil. Mag. (6), 50, 399, (1925).
2. O. Baudisch, Science, 77, 317 (1933).
3. O. Baudisch and W.H. Albrecht, J. Am. Chem. Soc., 54, 943 (1932).
4. W.P. Davey, Phys. Rev. (2), 21, 716 (1923).
5. P.H. Emmett and K.S. Love, J. Phys. Chem., 34, 41 (1930).
6. I.S. Jacob, J. Appl. Phys., 40, 920 (1969).
7. R.H. Ranger, FIAT Final Report No.923, (1947).
8. M. Sittig, Editor, Magnetic Materials, 9, (1970).
9. J. Robin, Bull. Soc. Chim., 1078-84, (1953).
10. T.S. West, Recent Developments in Inorg. & Org. Analytical Chemistry, Royal Institute of Chemistry Lectures and Monographs, 1959. No.1.
11. R.A. Brown and S.C. Bevan, J. Inorg. Nucl. Chem., 28(2), 389 (1966).
12. C.V. Ganapathy, S.M. Khuller, & Mrs. R. Ramachandran, Indian Patent No. 114829 (dt. 26.3.1969).
13. Lakhbir Singh, A.M. Chavan and A.N. Kotasthane, Indian Patent No. 131606.
14. J.W. McBain and A.M. Bakr, J. Am. Chem. Soc., 48, 690 (1926).

15. Lakhbir Singh, J. Sci. Industr. Res., 11A, 63 (1952).

16. D.A. Anderson and E.S. Freeman, Nature, 195, 1297 (1962).

17. W. Lodding and L. Hammell, Anal. Chem., 32, 6, 660 (1960).

18. A. Simon, H.J. Hermann and R. Schrader, J. Prakt. Chem., 30(3-4), 173 (1965).

19. K. Inouye, S. Ishii, K. Kaneko and T. Ishikawa, Z. Anorg. Allgen. Chem., 391, 86-96 (1972).

20. L. Erdey, Proc. Conf. Appl. Phys.-Chem. Methods of Chem. anal., Budapest, 3, 421-8 (1966).

21. B.R. Arora, N.K. Mandal, R.L. Choudhury, N.C. Ganguli and S.P. Sen, Technology, 9, 143(2-3), (1972).

22. S. Mukherjee and H. Roy, Technology, 3(2), 63 (1966).

23. Sastri, Indian J. Technology, 9(11), 439 (1972).(71)

24. P.L. Gunther and H. Rehaag, Z. Anorg. Allgem. Chem., 243, 60 (1939).

25. E.D. Macklen, J. Inorg. Nucl. Chem., 29, 1229 (1967).

26. R. Derie, M. Ghodsi and C. Calvo-Roche, J. Thermal Analysis, 9, 435 (1976).

27. I. David and A.J.E. Welch, Trans. Faraday Soc., 52, 1642 (1956).

28. E.J.W. Verway, Z. Krist., 91, 65 (1935).

29. Rathenau, Philips. Res. Rep., 1, 239 (1946).

=====

P A R T - II:

CHAPTER - I : INTRODUCTION

INTRODUCTION

Aluminium in the form of its oxide is among the most abundant elements of the earth's crust. It generally occurs as alumino-silicate. Free and pure alumina, however, is comparatively a rare mineral. It is found as corundum and emery in which it is associated with other oxides, such as Fe_2O_3, TiO_2, SiO_2 and Cr_2O_3. Transparent and pure alumina is also found in nature as white sapphire but in very small quantity. Transparent alumina crystals are also found in the coloured varieties, such as blue and yellow sapphire. The red variety is called the ruby and it is found in nature in various shades, such as rose, medium red and pigeon-blood shades. On account of their brilliance and ever-lasting polish, these sapphires and rubies are highly prized as gemstones for jewellery.

On account of extreme hardness, crystalline high purity alumina has become one of the most important technical materials in recent years. Many different kinds of electrical insulators, capacitors, dielectrics and printed circuit substrates are made by sintering high purity alumina.[1] It is also manufactured in the transparent single crystal form called synthetic gemstones. These are grown by a flame-fusion technique developed by A. Verneuil.[2] Although synthetic sapphire and ruby were originally manufactured

for jewellery, they soon found extensive industrial uses on account of their extreme hardness. These are used as jewel bearings for watches, meters and are also used for making long-lasting gramophone needles. On account of these industrial uses, manufacture of synthetic gemstones has become an important industry. It has a strategic value as well as about a Pound of synthetic jewel bearings go into the control units of one aeroplane.

Synthetic corundum or alpha (α) Al_2O_3 is one of the most important technical monocrystal. Its hardness is 9 on Mohs scale i.e. it is only next to diamond in this property. As it is very hard, it is resistant to wear and retains its polish against scratching. It is also resistant to chemicals and it has a low thermal expansion coefficient. Latest development in properties of ruby single crystals has been the generation of powerful "laser" beams.

For the manufacture of synthetic sapphire and ruby, we need high purity alumina. Besides purity, the alumina required for this purpose should have a transition structure. It is known that when amorphous gel type hydrated alumina is heated it passes through various structures before attaining the stable α-alumina structure at 1200°C. These transition stages are commonly known as the gamma (γ) alumina. Calcination of ammonium alum was chosen from several preparation methods, because it readily crystallizes from water

solution thus helping purification. Although there are some methods of preparation described in literature[3,4] producing alumina from ammonium alum, very few details are available about this process. In order to obtain high purity alumina it is important that alum should be extremely pure and can easily be achieved through successive crystallizations. Ammonium alum when heated to 1000°C is converted to a gamma type alumina[5] having a very fine particle size in the submicron range. This fine particle size is helpful in suspending it in oxygen supply of an oxy-hydrogen burner. The transition form of alumina also is helpful for single crystal growth as each particle does not become the seed as would happen if alpha alumina is used.

CHAPTER - II : METHOD OF PREPARATION OF HIGH PURITY ALUMINA

METHOD OF PREPARATION

2.A Preparation of Ammonium Alum :

Ammonium alum of high purity was prepared from reagent grade ammonium sulphate and aluminium sulphate. Ammonium sulphate solution was prepared by dissolving 510 g. in 2 litres of cold distilled water. Aluminium sulphate solution contained 2570 g. in 11 litres of hot water at 80°C. These concentrations are based on the solubility data given by David Schlain.[6] These solutions were filtered as such and mixed together with vigorous stirring when the following reaction takes place :

$$(NH_4)_2SO_4 + Al_2(SO_4)_3.18H_2O + 6H_2O \longrightarrow (NH_4)_2SO_4 \cdot Al_2(SO_4)_3 \cdot 24H_2O$$

or

$$2NH_4 \cdot Al(SO_4)_2 \cdot 12H_2O \quad \ldots\ldots (1)$$

As the solubility of ammonium alum is less than that of ammonium sulphate and aluminium sulphate, small crystals of the alum appear soon after mixing. These crystallites were allowed to grow with cooling of the mass to 10°C. In about six hours 1770 g. of the alum was obtained which was separated from the mother liquor by filtration.

The product was redissolved in 6.3 litres of distilled water at 80°C, filtered and recrystallized by cooling with mild agitation. Crystals were washed with cold water two or three times and air dried.

Analysis :

Iron and silica are the two likely impurities in ammonium alum which have to be reduced to the bearest minimum in the extra pure quality. These are analysed by standard method of colorimetry[7] using 1,10 phenanthroline and ammonium molybdate reagents respectively. It was found that recrystallized alum contained < 10 ppm of iron and silica. The overall purity was found to be 99.99 %.

2.B Calcination of Ammonium Alum to Alumina :

When white crystalline powder of ammonium alum is heated, it first loses water of crystallization and thereafter it decomposes in two stages giving off NH_3 and SO_3 leaving behind finely divided Al_2O_3.

(a) $(NH_4)_2SO_4.Al_2(SO_4)_3.24H_2O \xrightarrow{200^\circ C} (NH_4)_2SO_4.Al_2(SO_4)_3$

(b) $(NH_4)_2SO_4.Al_2(SO_4)_3 \xrightarrow{500^\circ C} Al_2(SO_4)_3 + 2NH_3 + SO_3 + H_2O$

(c) $Al_2(SO_4)_3 \xrightarrow{1000^\circ C} Al_2O_3 + 3SO_3$

The crystals of ammonium alum were placed in a vitrosil-silica dish and calcined in a muffle furnace. The temperature was raised gradually to 1000°C in 4 to 5 hours and held for about 3 hours. The product was an extremely fluffy and porous mass. It was lightly crushed to break the aglomerates and passed through a 325 mesh sieve. This extremely fine powder was identified by X-ray diffraction as gamma alumina (γ-Al_2O_3).

When gamma alumina is further subjected to heating it gets converted to the stable form alpha alumina (α-Al_2O_3) at about 1250°C.

CHAPTER - III : PHYSICO-CHEMICAL STUDIES

PHYSICO-CHEMICAL STUDIES

3.A Thermogravimetric and Differential Thermal Analysis of Ammonium Alum Decomposition :

Ammonium alum is generally calcined at 1000°C in one operation. This technique no doubt produces alumina in the desired ultrafine form. Nevertheless, it would be of scientific interest to investigate the various steps through which this decomposition proceeds.

Typical TGA and DTA curve of ammonium alum at the heating rate of 10°C per minute obtained with the help of a derivatograph unit (Type OD-102 MOM-Budapest) is shown in Fig. 1.

From the TGA curve it is seen that the dehydration of ammonium alum takes place in three distinct stages. The first step of water loss starts as early as 75°C and is complete by about 100°C. It is immediately followed by the second step which constitutes the major portion of dehydration and it takes place between 100°-200°C. The last portion of dehydration consists of a small narrow step at 200°-205°C. These steps also correspond to distinct and sharp endothermic peaks in the DTA curve.

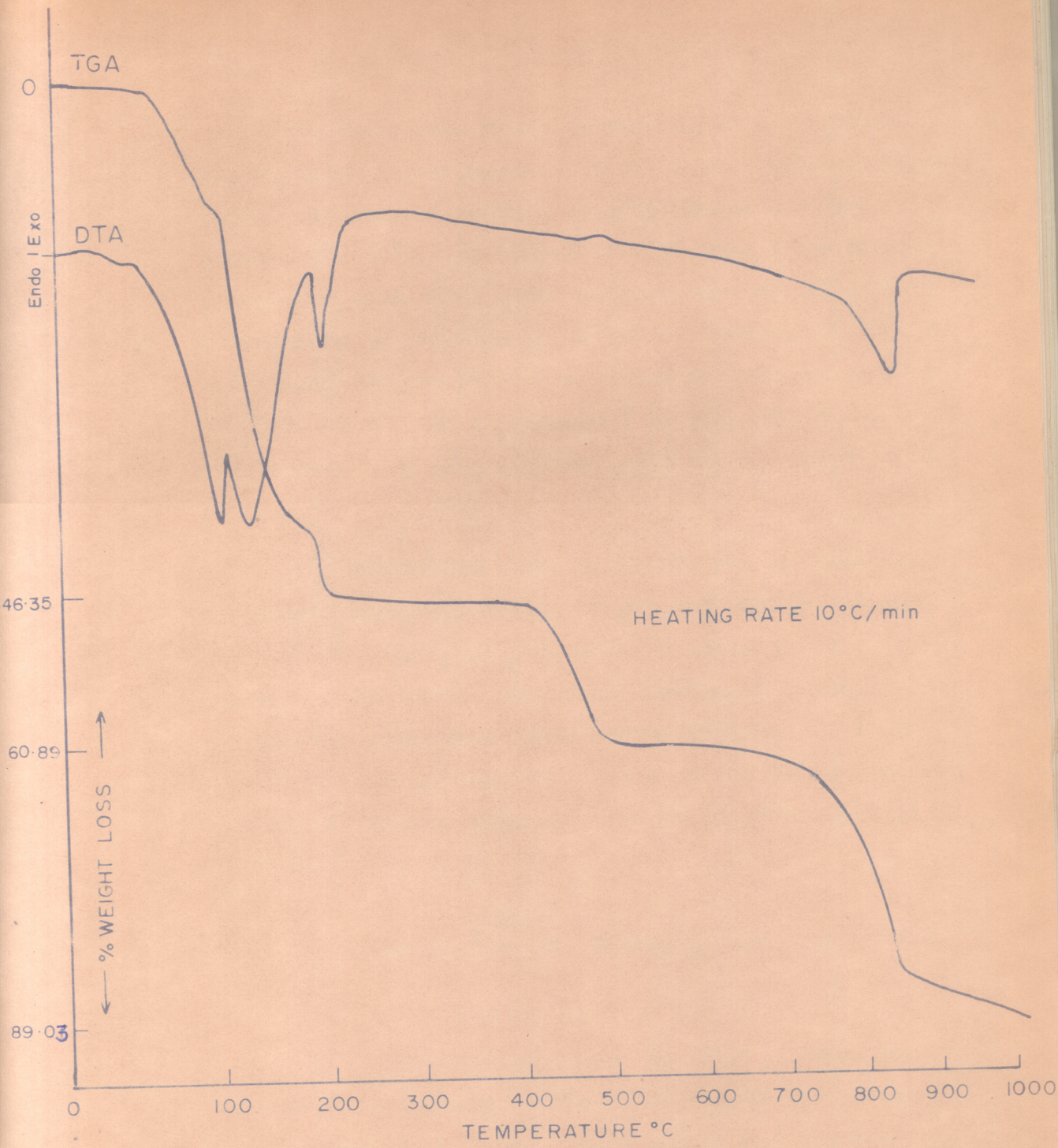

FIG. 1: TGA AND DTA OF AMMONIUM ALUM IN AIR

The first step in the dehydration of $(NH_4)_2SO_4 \cdot Al_2(SO_4)_3 \cdot 24H_2O$ corresponds to 11.85 % loss, which indicates that 6 molecules of water of crystallisation are lost between 75°-100°C. The second step in which major portion of water is lost shows about 31 % loss corresponding to 16 molecules of water which are driven off between 100°-200°C, and finally the remaining 2 molecules of water are lost at 200°C to 205°C. The observed 46.3 % total dehydration weight loss is in good agreement with the calculated value of 47.7 %.

The dehydration stage in TGA and DTA is followed by an almost horizontal portion between 205°-405°C, showing that anhydrous $(NH_4)_2SO_4 \cdot Al_2(SO_4)_3$ is stable in this wide range of about 200°C. On further heating it decomposes in two steps. Ammonium sulphate decomposes from 405° to 500°C. The observed weight loss of 14.54 % for the loss of ammonium sulphate is in good agreement with the theoretical value of 14.57 %.

$$(NH_4)_2SO_4 \cdot Al_2(SO_4)_3 \xrightarrow{500^\circ C} Al_2(SO_4)_3 + 2NH_3 + SO_3 + H_2O \quad \ldots\ldots (2)$$

It is interesting to note that this decomposition appears as just a kink in the DTA tracing on the exothermic side. Normally it is expected to appear as a sizable endothermic peak, as in the next step representing decomposition of aluminium sulphate. This observation indicates

that probably the liberated NH_3 gas burns in air at this temperature thus compensating for the heat absorbed during decomposition.

Aluminium sulphate is stable between 500°-600°C and starts decomposing appreciably around 650°C loosing sulphur trioxide. The rate of weight loss becomes fast at about 800°C and is complete at about 860°C. The DTA curve also shows a distinct endothermic peak at about 850°C.

$$Al_2(SO_4)_3 \xrightarrow{650^\circ - 860^\circ C} Al_2O_3 + 3\,SO_3 \qquad \ldots\ldots (3)$$

The final total weight loss of 89.03 % is in agreement with the calculated value of 88.75 %.

$$(NH_4)_2SO_4.Al_2(SO_4)_3.24H_2O \longrightarrow Al_2O_3 + 2NH_3 + 4SO_3 + 25H_2O \qquad \ldots\ldots (4)$$

The product obtained from the calcination of ammonium alum was found to be a very light fluffy mass of gamma alumina which was lightly crushed and sieved.

3.B Surface Area Measurement :

3.B.1 B.E.T. Apparatus

The surface areas are determined by using B.E.T. apparatus shown in Fig. 2. It consists of three gas

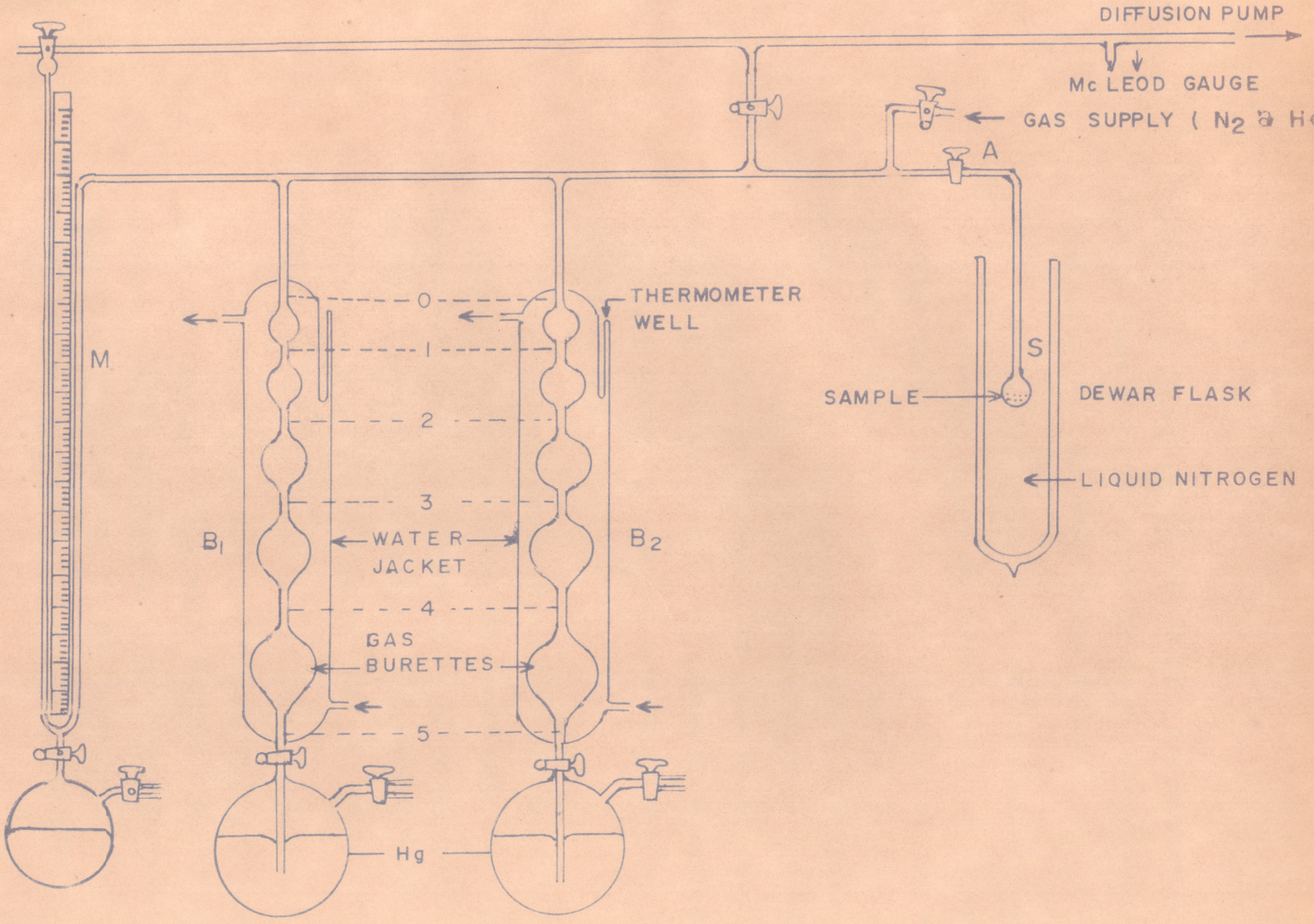

FIG. 2 : GAS ADSORPTION UNIT FOR THE MEASUREMENTS OF BET SURFACE AREA

burettes B_1, B_2 and B_3 (B_3 not shown), sample bulb S, mercury manometer M, nitrogen and helium gas reservoirs and a pumping system (not shown in the figure).

The burettes consist of a series of bulbs of progressively diminishing volume and connected to each other by capillary tubing. The volumes of the bulbs between successive reference marks are accurately determined by weighing mercury taken out from each one of them. The burettes are surrounded by water jackets. A thermowell is provided for the measurement of temperature of water in the burettes. Nitrogen gas was purified by the conventional methods.[8] Pure helium gas supplied by the British oxygen Co., London was used as such.

For the measurement of surface area about 0.2-0.3 gms. of alumina was filled in the adsorption bulb and weighed before sealing to the system. The dead space volume (V_o), is the volume between stopcock A, the zero reference marks on the burettes and the manometer and was determined by using pure helium gas.

The free space in the adsorption bulb, that is, the space not occupied by the solid was then determined as follows. A dose of helium gas was taken and its volume was determined by compressing the gas successively in the burette bulbs and simultaneously noting the pressure.

The adsorption bulb was then immersed in liquid nitrogen bath and stopcock A was opened to admit helium into the adsorption bulb. The new pressure P_1 was noted. At different reference points, pressures were noted as before and the bulb factor V_A was calculated. Helium gas was pumped off and the evacuation continued till a vacuum of 10^{-6} mm of Hg was obtained, and then stopcock A was closed. A dose of nitrogen gas was calibrated as before and then admitted to the adsorption bulb immersed in liquid nitrogen. The gas was adsorbed on alumina and the pressure in the system gradually dropped. After equilibrium is attained the pressure in the system was noted. The temperature of the burettes and the position of the mercury in them were noted. The mercury level in the burette was successively raised and the equilibrium pressure attained was recorded at the reference mark. Fresh dose of nitrogen was admitted and calibrated as before. Adsorption measurements were carried out till sufficient number of points at different pressures were obtained.

If V_1 is the volume at NTP of nitrogen taken, V_2 the volume remaining in the system upto stopcock A and V_3 the volume in the adsorption bulb, then

$$V_{adsorbed} = V_1 - V_2 - V_3 \left(1 + \frac{\alpha P}{760}\right),$$

where α is the correction for non-ideality of nitrogen at $78^{\circ}K$.

Surface area was determined by using the BET equation.

$$\frac{P}{V_{ads}(P_o - P)} = \frac{1}{V_m C} + \frac{(C-1)}{V_m C} \cdot \frac{P}{P_o}$$

$$\left(C = e^{E_1 - E_l / RT} \right)$$

where V_m = volume of nitrogen necessary to form a monolayer, P_o is the saturated pressure of the nitrogen at $78^{\circ}K$, C is a constant which depends upon the adsorbate-adsorbent system. A plot of $\frac{P}{V_{ads}(P_o - P)}$ against $\frac{P}{P_o}$ gave a straight line. From the slope and intercept of the line and the weight of the alumina taken, the surface area of alumina was calculated using the equation :

$$SA(m^2/gm) = \frac{4.38}{(\text{slope} + \text{intercept})} \cdot \frac{1}{\text{wt. of alumina}}$$

3.B.2 Adsorption of Nitrogen and Surface Area of Alumina :

The amount of nitrogen adsorbed in mls. per gm. at NTP on alumina at various pressures and the calculated surface areas are given in Table-1. It is seen from the table that 1 g. gamma Al_2O_3 sorbs about 84.0 mls. of nitrogen at a pressure of 210 mm, while alpha alumina adsorbs only 33.25 mls.

TABLE - 1

Sr. No.	Sample temperature and time	BET surface area (M^2g^{-1})	mls. (at STP) of nitrogen adsorbed per gram of γ-Al_2O_3 at pressures (mm of Hg)										
			30	40	60	80	100	120	140	160	180	200	210
1	γ-Al_2O_3	274.5	38.5	44.0	49.5	52.5	56.0	60.0	64.5	68.0	74.0	81.0	84.0
2	γ-Al_2O_3 300°C, 5 hrs.	251.5	-	52.0	62.0	65.5	69.0	72.0	74.0	75.5	77.0	77.5	77.5
3	γ-Al_2O_3 400°C, 5 hrs.	187.5	-	-	42.0	45.0	48.0	51.0	54.5	57.5	60.0	64.5	65.5
4	γ-Al_2O_3 500°C, 5 hrs.	170.5	-	32.0	36.0	37.5	40.0	42.0	44.0	46.0	48.0	50.0	51.0
5	γ-Al_2O_3 600°C, 5 hrs.	162.25	30.0	34.0	36.0	37.5	39.5	41.0	43.0	45.0	46.5	48.5	49.0
6	γ-Al_2O_3 700°C, 5 hrs.	151.97	-	19.0	27.5	31.5	33.0	34.5	35.5	36.75	38.0	39.0	39.5
7	γ-Al_2O_3 1000°C, 1 hr.	129.10	25.0	27.5	28.2	29.0	30.0	31.0	32.0	33.0	33.5	34.5	35.0
8	α-Al_2O_3 1200°C, 1 hr.	102.20	-	15.0	23.2	25.0	26.0	27.5	28.5	29.5	31.0	32.5	33.25

The amount adsorbed per gm. increases with increasing pressure and decreases with the activation temperature. The latter may be attributed to the sintering behaviour of gamma Al_2O_3.

3.C X-ray Diffraction Studies :

The alum are a series of a double salts which may be expressed as[9]

$$R^{i}\ R^{iii}\ (R^{iv}\ O_4)_2 \cdot 12H_2O$$

in which R^{i} is monovalent cation, R^{iii} a trivalent metal and R^{iv} is generally sulphur. The representative powder diffraction pattern for ammonium alum with observed lattice spacings (d $\mathring{A}$) and the ASTM values are summarised in Table-2.

Thermal decomposition of ammonium alum yields a crystalline variations of alumina at different temperatures which are transition stages in a process eventually yielding corundum (α-Al_2O_3). The sequence of these transformations have been fairly well known for a number of years.

The data represented in Table-2 for gamma and alpha-alumina are in good agreement with data of Stumpf.[10]

The metastable γ-Al_2O_3 has been assigned[11] a defect spinel structure $Al_{21\frac{1}{3}}O_{32}$, that is $21\frac{1}{3}$ metal atoms are arranged at random in the sixteen octahedral and eight tetrahedral positions of the spinel structure.

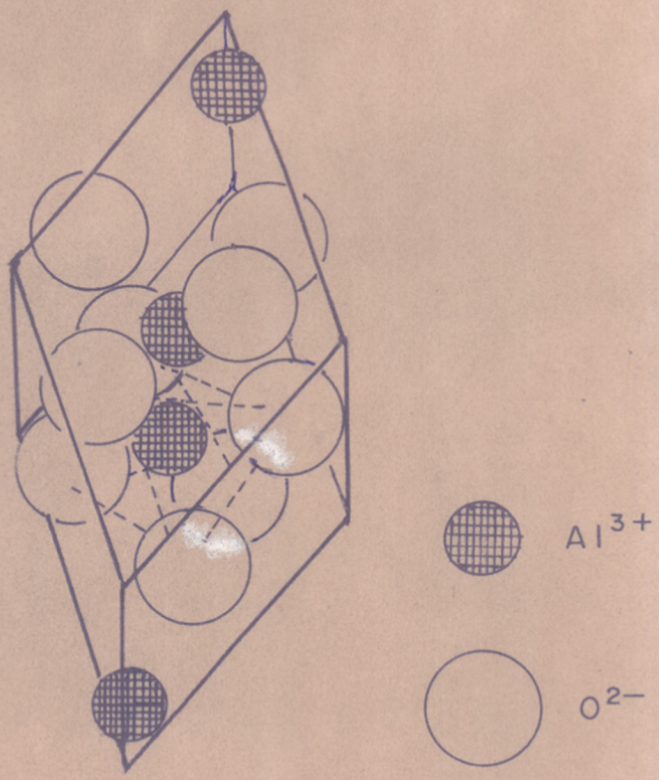

FIG. 3. LATTICE STRUCTURE OF α-Al_2O_3 (After Zachariasen)

TABLE - 2

Lattice spacings and intensities for ammonium alum, γ- and α-Al_2O_3 (Cu-Kα radiation)

Ammonium Alum $(NH_4)_2SO_4.Al_2(SO_4)_3.24H_2O$			Gamma Alumina γ-Al_2O_3			Alpha Alumina α-Al_2O_3		
$I_{obs.}$	d Å		$I_{obs.}$	d Å		$I_{obs.}$	d Å	
	observed	ASTM 2-0490		observed	ASTM 2-1420		observed	ASTM 5-0712
MW	5.96	6.09	MS	2.73	2.80	MS	3.46	3.479
MS	5.37	5.43	MS	2.37	2.39	VS	2.54	2.552
MS	4.28	4.30	W	2.26	2.28	MW	2.36	2.37
MS	4.00	4.05	S	1.97	1.98	VS	2.07	2.085
M	3.82	3.84	VW	1.80	1.82	MW	1.73	1.74
W	3.65	3.67	VVW	1.61	1.62	S	1.59	1.601
VS	3.23	3.25	M	1.51	1.52	VVW	1.53	1.54
MS	3.00	3.04	VS	1.39	1.40	W	1.40	1.40
M	2.81	2.79	M	1.11	1.14	MW	1.36	1.37
M	2.70	2.72	M	0.10	0.99	VW	1.22	1.239
MW	2.57	2.59	MS	0.79	0.808			
W	2.46	2.47						
M	2.34	2.36						
MW	2.07	2.10						
MS	1.95	1.97						
S	1.91	1.92						

VS = very strong
MS = medium strong
S = strong
M = medium
MW = medium weak
W = weak
VW = very weak
VVW = very very weak

Only alpha-alumina (α-Al_2O_3) has a definitely established structure. The crystallographic structure of alpha-alumina has been determined by W.H. Zachariasen. Fig. 3 depicts the position of Al and O atoms in the lattice. For simplicity, one can figure out that oxygen atoms form the close hexagonal packing in which small aluminium atoms are distributed at the octahedral holes. It may be seen that each Al atom is surrounded by six O atoms, three below and three above.

REFERENCES

REFERENCES

1. G.C. Martin, Ceramics, 9, 114, (1958).
2. A. Verneuil, Compt. Rend., 135, 791 (1902); ibid, 151, 1063 (1911).
3. S. Ino, J. Chem. Soc. Japan, Industr. Chem. Section, 58, 181-83 (1955).
4. S. Okada, K. Kuwashima, Kogyo Kagaku Zasshi, 59, 1301 (1956).
5. W.G. Burgers, A. Claassen and I. Zerlike, Z. Physik, 74, 593-603 (1932).
6. S. David, J.D. Prater and S.F. Ravitz, Industr. Eng. Chem., 39(1), 74 (1947).
7. A. Vogel, 'Text Book of Quantitative Inorg. Analysis', 3rd Edition, pp.786, 909 (1961).
8. L.G. Joyner, 'Scientific and Industrial Glass Blowing and Laboratory Techniques' , Ed. W.E. Barr, p. 257 (1949).
9. H. Lipson, Proc. Roy. Soc., 148A, 664 (1935); ibid., 151A, 347 (1935).
10. H.C. Stumpf, A.S. Russell, J.W. Newsome and C.M. Tuker, Industr. Eng. Chem., 42(7), 1398 (1950).
11. A.F. Wells, 'Structural Inorganic Chemistry', 3rd Edition, Clarendon Press, Oxford, (1961).

=====

SUMMARY

SUMMARY

The work presented in this thesis consists of two parts and each part is comprised of three chapters.

The first part of the thesis relates to the preparation of and physico-chemical studies on Gamma Ferric Oxide.

Preparation of Gamma Ferric Oxide

Gamma ferric oxide was prepared by two methods : (i) the ferrous oxalate process and (ii) the ferric oxide hydrate process.

In the first method ferrous oxalate dihydrate was at first decomposed by heating to ferrosoferric oxide Fe_3O_4 and then oxidised to gamma ferric oxide. This decomposition of ferrous oxalate is generally carried out in an inert atmosphere at a temperature of 700°-800°C. During this investigation it was found that the temperature of ferrous oxalate decomposition can be brought down to as low a temperature as about 450°C when it is carried out in an atmosphere of steam. This observation has applied value as at this low temperature no sintering of particles takes place. It is also found that the spinel structure of Fe_3O_4 is stabilised or facilitated in the presence of moisture. The oxidation of Fe_3O_4 to gamma ferric oxide has also been

carried out with moist mass when the conversion could be completed at 250°C in air-oven. Water vapours appear to play an important role in stabilising the gamma ferric oxide inverse spinel structure. The product obtained by this method is of submicron particle size having spherical shape which is known as the 'equant' form.

Gamma ferric oxide was also prepared from ferric oxide hydrate (α-FeOOH) in the needle shape particles known as the acicular form. The alpha ferric oxide hydrate was precipitated at a very slow rate by passing air through ferrous sulphate solution in the presence of scrap iron. The yellow precipitate of α-FeOOH thus obtained was decomposed to ferrosoferric oxide (Fe_3O_4) at about 400°C in a reducing atmosphere of hydrogen. It was then oxidised as before to gamma ferric oxide. The acicular needle shape in this process originates in the slow growth of ferric oxide hydrate crystallites along the preferential crystal axis. This shape is retained if their reduction to Fe_3O_4 and reoxidation to γ-Fe_2O_3 is carried out under controlled conditions. Retention of the spinel structure of Fe_3O_4 in the gamma ferric oxide is made possible by the fact that this conversion requires only about 3 % additional oxygen in the structure.

Thermal analysis

The thermogravimetric analysis of ferrous oxalate dihydrate showed two discrete steps in nitrogen and hydrogen atmosphere. However, a single sharp step was observed in oxygen. The DTA analysis in air also showed a single peak. This is because the liberated CO immediately gets oxidised to CO_2 which is exothermic in nature and leads to completion of decomposition.

Thermogramsof alpha ferric oxide hydrate in air and H_2 showed two steps. However, in air the slow weight loss was exhibited in the second step. This is attributed to loss of oxygen forming Fe_3O_4. Although the dehydration of ferric oxide hydrate takes place at much lower temperature than expected, it is believed to be due to the small particle size in the submicron range. In H_2 atmosphere it was observed that ferric oxide hydrate directly gets converted to Fe_3O_4 in a single step. However, the Fe_3O_4 formed was stable only in a very narrow range of temperature above ($> 400^{o}C$) which it starts reducing to metallic iron.

DTA studies of Fe_3O_4 oxidation in air showed two exothermic peaks the first peak corresponding to the formation of gamma ferric oxide followed immediately by another exothermic peak corresponding to the phase transformation from gamma $\longrightarrow$ alpha form.

The morphology of the original crystals (α-FeOOH) remains unaltered throughout the entire process of reduction and reoxidation of ferric oxide hydrate. This was confirmed by electron microscopy which showed elongated needle shaped particles with diameters less than one micron and length to width ratio of about 10:1 to 20:1.

Magnetic properties of γ-ferric oxide

A detailed investigation of the magnetic properties of Fe_3O_4 and γ-Fe_2O_3 such as saturation magnetization and magnetic hysteresis (B-H) loop studies were carried out. The compound Fe_3O_4 oxidised at various temperatures from 155° to 250°C which showed a steady decrease in saturation magnetization till it formed γ-Fe_2O_3.

X-ray diffraction studies

The X-ray results from powder patterns supported the earlier reports that Fe_3O_4 and γ-Fe_2O_3 have identical structures.

The second part of the thesis deals with the preparation and physico-chemical studies on high purity aluminium oxide.

Preparation of high purity alumina

The preparation of ultra pure aluminium oxide occupies a central role in growing single crystals of synthetic

sapphire and for electronic purposes. Most suitable starting material chosen for this purpose was ammonium alum, which can be easily purified by crystallization and transferred on calcination at 1000°C to an extremely fine particle size and low density alumina.

High purity ammonium alum was prepared by mixing equivalent quantities of reagent grade ammonium sulphate and aluminium sulphate as almost saturated solutions in distilled water at 80°C. Crystals appeared immediately on mixing which grew further during cooling. Only two crystallizations were required to attain the desired degree of purity.

The most likely impurities of iron and silica in the ammonium alum were tested colorimetrically with 1,10-phenanthroline and ammonium molybdate reagents. These impurities were found to be present in very small quantities (< 10 ppm).

Thermal properties

The thermogram of ammonium alum at the heating rate of 10°C per minute in air showed that its dehydration takes place in three distinct stages from 75° to 205°C. This indicates that all the 24 molecules of water of crystallization do not have the same ionic surroundings in the crystal. DTA also showed similar results. The TGA and DTA studies

also revealed that decomposition of $(NH_4)_2SO_4$ and $Al_2(SO_4)_3$ components takes place at two distinct and separate stages. Ammonium sulphate decomposed at 405°-500°C, while aluminium sulphate was observed to decompose at 650°-860°C.

For large scale preparation the calcination of ammonium alum was carried out in silica dishes at 1000°C in a muffle furnace. The product was identified as gamma alumina by X-ray diffraction. When gamma alumina was further subjected to heating upto 1250°C, it was found to undergo crystalline modifications culminating in the stable alpha form.

Nitrogen adsorption

The specific surface areas of γ- and α-Al_2O_3 were measured by nitrogen adsorption using BET apparatus. It was observed that gamma alumina adsorbs 2.5 times more nitrogen than alpha alumina.

=====